Numerical analysis of a photonic crystal fiber-based biosensor for the detection of Vibrio Cholera and Escherichia Coli bacteria in the THz regime

Dana N. Alhamss[1], Sofyan A. Taya[1*], Abdulkarem H. M. Almawgani[2], Ayman Taher Hindi[2], Anurag Upadhyay[3], Shivam Singh[4], Ilhami Colak[5], Amrindra Pal[6], Shobhit K. Patel[7]

[1]Physics Department, Islamic University of Gaza, P.O. Box 108, Gaza, Palestine.
[2]Electrical Engineering Department, College of Engineering, Najran University, Najran, Kingdom of Saudi Arabia.
[3]Department of Applied Science & Humanities, Rajkiya Engineering College, Azamgarh, U. P., India.
[4]Department of Electronics & Communication Engineering, ABES Engineering College, Ghaziabad, U.P., India.
[5]Department of Electrical and Electronics Engineering, Nisantasi University, Istanbul, Turkey.
[6]DIT University, Department of EECE, Dehradun, Uttarakhand, India.
[7]Department of Computer Engineering, Marwadi University, Rajkot-360003, India.

*Corresponding author
Email: staya@iugaza.edu.ps

Abstract

To ensure good water quality, microbiological contamination in water must be detected. This process is made easier and more distinctive by using a photonic crystal fiber (PCF), which offers outstanding optical sensing capabilities. In this work, a PCF sensor model is proposed for detecting two types of waterborne bacteria, namely Vibrio Cholera, and Escherichia Coli bacteria. The core region of the proposed PCF sensor is made up of a single rectangle and the cladding region has 32 rectangular air holes that have the same height and width as the core rectangle. Zeonex is employed as the fiber material. Using Comsol 5.6 which is based on the finite element method, the model is numerically analyzed and structured. The simulation verifies the effectiveness of the proposed PCF to detect the analyte samples. Numerous performance indicators are calculated at an operating of 2.8 THz. Simulation results show that the proposed PCF sensor is promising. Extremely high relative sensitivity (97.996%), lower effective area (6.3575×10^4 μm^2), higher numerical aperture (0.23319), lower effective material loss (0.0034 cm^{-1}), and lower confinement loss (0.1×10^{-14}) have been obtained which indicate an efficient PCF sensor. Additionally, the simplicity of the PCF design ensures the fabrication possibilities of the proposed sensor.

Keywords: Photonic crystal fiber; Biosensor; Vibrio Cholera; Escherichia Coli; Relative sensitivity.

1. Introduction

Water consumption has been rising at a rate of 1% per year for the past 50 years in tandem with the expansion in the world's population. By 2050, it is expected to rise by another 20–30% [1]. In contrast, the availability of safe drinking water and its quality are steadily decreasing as a result of environmental pollutants, and agricultural, industrial, and residential issues. This can lead to serious health risks to both people as well as animals [2]. Particularly, exposure to microbiological pollutants, such as protozoa, viruses, and bacteria, is associated with increased respiratory problems, intestinal diseases, fever, dehydration, and diarrhea, which can sometimes be fatal. Currently, 2.1 billion people

lack access to safe drinking water, and each year, approximately 2 million people, mostly children, die as a result of contaminated water sources and sanitary conditions [3]. As global freshwater shortage increases, water recycling, specifically treated wastewater reclamation, becomes more crucial. Kuwait and Qatar are at the top of the list for the most frequent water reuse, with >85% of their wastewater being treated and recycled [4]. Along with the obvious benefits, there is an increasing concern about pathogens from reclaimed wastewater contaminating surface and groundwater. Therefore, it is essential to continuously monitor the quality of both drinking water and reclaimed water. Identification and detection of microorganisms in water are usually based on molecular biology and microbiology techniques. These methods include microscopy examination, staining, microarray, cell culture techniques, membrane filtration, and others [5]. The aforementioned techniques are regarded as reliable but, particularly in the case of bacteria, have several drawbacks, such as the necessity of concentrating the bacteria by membrane filtration of large amounts of water, lengthy growth lag times (up to 72 h), the requirement for trained and highly skilled personnel, and the high costs [6].

Photonic crystals are nanostructured materials that manipulate the flow of light in a manner analogous to how semiconductors control the flow of electrons. They exhibit periodic variations in refractive index, typically on the scale of the wavelength of light, creating bandgaps where certain wavelengths cannot propagate. There are several types of photonic crystals, including one-dimensional (1D), two-dimensional (2D), and three-dimensional (3D) structures. Each type has unique properties and applications. One-dimensional photonic crystals consist of alternating layers with different refractive indices and are often used in optical coatings and mirrors. Two-dimensional photonic crystals feature a periodic pattern in two dimensions, offering control over light in-plane, and are employed in microcavity lasers and waveguides. Three-dimensional photonic crystals provide full control over light in all directions and are utilized in creating optical integrated circuits, sensors, and even novel light sources like LEDs and lasers. These versatile materials find applications in optical communication, sensing, imaging, and emerging technologies, making them an integral part of photonics research and development.

Here, a technique for utilizing photonic crystal fiber (PCF) to detect waterborne bacteria is proposed. Researchers have recently paid a lot of attention to PCF-based chemical and biological sensing and detection. The PCF is a form of optical fiber. It provides some outstanding features such as maintaining negligible confinement loss (CL) and dispersion [7], along with higher nonlinearities [8]. CL and sensitivity are the two key guiding parameters for liquid and chemical detection. Birefringence is also a crucial property of PCF, and higher values of it are highly expected. This could be done by adding asymmetry to the fiber [9]. For many application fields, including detection, telecommunications, etc., higher PCF birefringence is highly praised [10]. Zeonex, Teflon, and Silica are few examples of the several fiber materials that can be used as bulk materials [11-14]. Zeonex's chemical properties have given them several advantages, making them unique and best suited. Zeonex is the finest option for fiber material because numerous studies have shown that it has greater chemical resistance. Several scholars have concluded that Zeonex has better chemical resistivity and as a result, it is the best option as a fiber material [15]. Several chemical and bio-sensors have so far been modeled using PCF. Arif et al presented a nonlinear PCF-based senor in 2019 [16]. The cladding region of the proposed PCF has hexagonally organized air holes, while the core is elliptical. To examine the effects of some design parameters, a thorough analysis covering a wide wavelength range (0.6 m–1.6 m) has been given [16]. This PCF has a CL of 2.17×10^{-12} cm^{-1} and a birefringence of 0.005. The sensor sensitivity is only 41%. Additionally, the effective material loss (EML) has not been calculated. A PCF of a similar type has been proposed by Leon et al. in 2020 [17]. The configuration of the cladding air holes is similar to that described in [16] with the core being four small circular holes. This sensor has a sensitivity of 49% and a somewhat higher birefringence of around 0.008. However, it has a greater CL and the EML has not been investigated. Another PCF with heptagonally organized air holes in the cladding region was proposed in 2019 [18]. It has shown

a slightly higher sensitivity (63.24%). However, for this PCF, the CL and effective area (EA) are higher. A PCF has been developed to detect NaCl [19]. The core region has four rectangular holes. An extremely high sensitivity of 91.5% has been obtained. A birefringence is 0.0027 has been attained. The proposed PCF has a reduced EML and CL. The drawback of this sensor is a relatively large EA, which leads to a low value of the numerical aperture. A PCF sensor for environmental contaminants was proposed [20]. The model reaches a sensitivity of about 90%. However, an EML of about 0.02 cm^{-1} was obtained. A PCF-based alcohol sensor has been recently presented [21] which achieved a sensitivity of about 92.3%. A rectangular core PCF structure to detect the major components of blood has been presented. Topas as bulk fiber material has been used due to its optical properties where Topas is a brand of cyclic olefin copolymer, a type of thermoplastic polymer. It is composed of repeating units of cyclic olefins and ethylene. Topas is known for its transparency, high chemical resistance, and low water absorption. It is used in various applications, including optical and microfluidic systems, due to its excellent optical and mechanical properties. Some key optical properties of Topas are transparency and low birefringence.

The proposed PCF has provided a relative sensitivity of about 94.38% [22]. The detection of blood and skin cancerous cells using a PCF-based sensor has been reported. The proposed sensor contains rectangular holes in the cladding and the core region has a single rectangle. Relative sensitivities of 96.74%, 96.56%, 96.61%, 96.34%, and 95.69% have been obtained for different cancerous cells [23]. All of these PCFs, along with a few other PCFs reported in [21–29], suggest that there is still room to model more PCFs. We seek a structure that is easy to fabricate, has higher sensitivity, has higher NA, and has lower EA, lower EML, and lower CL.

The main aim of this study is to numerically design and analyze a rectangular-hole PCF for detecting Vibrio Cholera (V. Cholera), and Escherichia Coli (E. Coli). To estimate the sensor performance, relative sensitivity, birefringence, CL, EA, and EML, are analyzed.

It is worth mentioning that replacing the rectangular air holes of the proposed PCF with circular or elliptical ones [30,31] can facilitate the fabrication process due to the drawbacks associated with rectangular air holes. In the current fiber technology, there are some difficulties in fabricating rectangular air holes PCF due to cost considerations. These holes (rectangular) are prone to fragility when subjected to lateral pressure during the fabrication process. Moreover, the shape and size of the air holes affect the mode field distribution within the PCF. Circular air holes tend to have a more symmetric mode profile, while elliptical holes introduce anisotropy, leading to asymmetric mode profiles. The mode field distribution directly influences the interaction between light and the surrounding environment. A change in the mode field distribution can impact the sensitivity of the PCF sensor. What encouraged us to work with rectangular-hole PCF is the high sensitivity obtained in this paper compared to that of other shapes as will be seen at the end of this paper.

The motivation for the detection of V. Cholera and E. Coli bacteria is primarily driven by public health concerns and the need to prevent and manage outbreaks of diseases associated with these bacteria. V. Cholera is the causative agent of cholera, a highly contagious and potentially deadly diarrheal disease. E. coli strains, particularly certain pathogenic variants like E. coli O157:H7, can cause severe foodborne illnesses. Detecting these bacteria is crucial to prevent the spread of these diseases and their associated health impacts. Cholera and E. coli infections can lead to large-scale outbreaks, especially in regions with inadequate sanitation and clean water resources. Timely detection helps public health authorities respond effectively to limit the spread of these infections and provide medical care to affected individuals. Both V. Cholera and pathogenic E. coli strains are often associated with contaminated water sources and food products. Detecting these bacteria in water supplies, food items, and agricultural products is essential to ensure the safety of the food and water we consume. In a clinical setting, the detection of V. Cholera and pathogenic E. coli strains is crucial for diagnosing and treating patients with bacterial infections. Rapid and accurate detection can lead to timely medical interventions.

The novelty of using the proposed PCF as a sensor for detecting two types of waterborne bacteria lies in its ability to offer a highly sensitive and versatile platform for this specific application. Using a PCF as a sensor enables the simultaneous detection of two types of waterborne bacteria, such as V. Cholera and E. coli. This dual detection capability is advantageous in scenarios where multiple bacterial contaminants need to be monitored concurrently. PCFs are known for their high sensitivity due to the strong light-matter interactions that occur within their microstructured cores. This enhanced sensitivity allows for the detection of even low concentrations of bacteria, enhancing the accuracy of water quality monitoring. PCF-based sensors can provide real-time monitoring of bacteria in water samples. This is crucial for early detection of bacterial contamination in drinking water sources, helping prevent waterborne diseases and ensuring public health.

2. Fabrication feasibilities and sensor model design

Sol-gel, extraction, stacking, and 3D printing [32,33] are a few popular techniques used today to fabricate PCF. Drilling and slurry casting can support the sub-micron scale fabrication [34]. Circular air hole fabrication can be done using stacking and sol-gel techniques. However, the fabrication of asymmetric PCF sensors, having rectangles, is perfectly suited to extraction and 3D printing techniques. These symmetric and asymmetric structures help in achieving the desired properties. According to Ebendorff-Heidepriem et al. [35], rectangular air holes have been fabricated.

We propose a PCF sensor which has rectangular air holes in the cladding region and a rectangular core. To fabricate such a PCF, we choose an appropriate background material. Zeonex is commonly employed as fiber material. After drawing the fiber, we create rectangular air holes in the cladding region. This can be done using techniques like drilling, chemical etching, or laser ablation. The specific method will depend on the material and the desired hole dimensions.

The finite element method (FEM) is employed to design and analyze the PCF sensor. There are several sequential steps involved in the designing and optimization of the model using FEM. First, a random PCF model is created. After that, materials are assigned to the regions of the core and cladding. Setting up the mesh and initializing the boundary conditions are the next step. Performance metrics are then extracted using partial differential equation solutions. These metrics are then analyzed and the results are checked carefully. The steps are repeated many times until standard results are obtained. A cross-sectional illustration of the proposed PCF is shown in Fig. 1a, where the yellow rectangle represents the core region in which the analyte is injected for sensing purposes, and a schematic diagram showing all the dimensions is shown in Fig. 1b in which we have adopted the following values: $w = 300\ \mu m$, $h = 500\ \mu m$, $\Lambda = 315\ \mu m$, $R = 1650\ \mu m$ and $r = 1518\ \mu m$, in a similar manner to Ref [36], where w and h are the width and height of the rectangles, Λ represents the distance between the centers of two successive rectangles, R stands for the radius of the entire fiber, and r is the radius of the whole fiber without the perfectly matched layer (PML). The PLM has a width of 132 μm. The electromagnetic signal that is propagating towards the surface is absorbed by the PML, and this is the main function of the PML shield. Figure 1c shows the meshing output of the proposed PCF. The normal mesh has been used and it is found to have 26670 domain elements and 3018 boundary elements. 32 rectangular air holes that have the same height and width as the core rectangle make up the cladding region. The distance (pitch) between any two adjacent rectangles is 15 μm. The fiber material used is called Zeonex. It exhibits reduced bulk absorption loss in the range of terahertz when compared to other materials like silicon, topas, etc. In the spectral range 0.1–10 THz, it has a refractive index (RI) of 1.53 and a bulk absorption loss of $\alpha_{Zeonex} = 0.2\ cm^{-1}$ [37-39]. Through the terahertz band, the RI of zeonex maintains almost the same value [36].

We have introduced pure water, V. Cholera, and E. Coli bacteria as an analyte in the core region. Figure 2 shows the light propagation through these analytes in the x and y directions. Loss is minimal since just a tiny fraction of the light travels outside of the core region. The black-red area shows the maximum light confinement. The intensity steadily drops off towards the core boundary and the red arrow indicates the direction in which light travels.

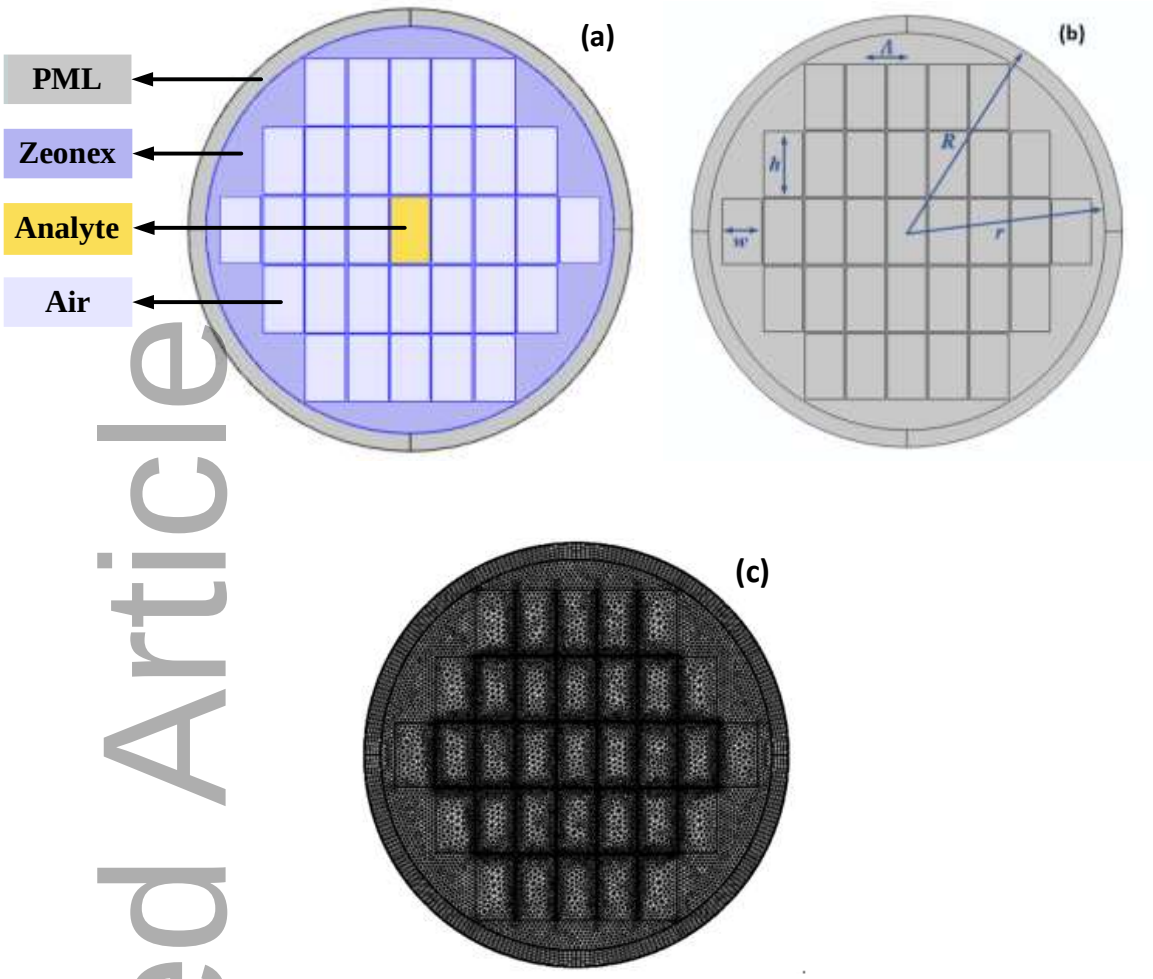

Fig. 1. (a) Cross-sectional representation of the proposed PCF sensor, (b) schematic diagram of the proposed PCF where, $w = 300\ \mu m$, $h = 500\ \mu m$, $\Lambda = 315\ \mu m$, $R = 1650\ \mu m$, $r = 1518\ \mu m$, (c) Meshing output with 26670 domain elements and 3018 boundary elements.

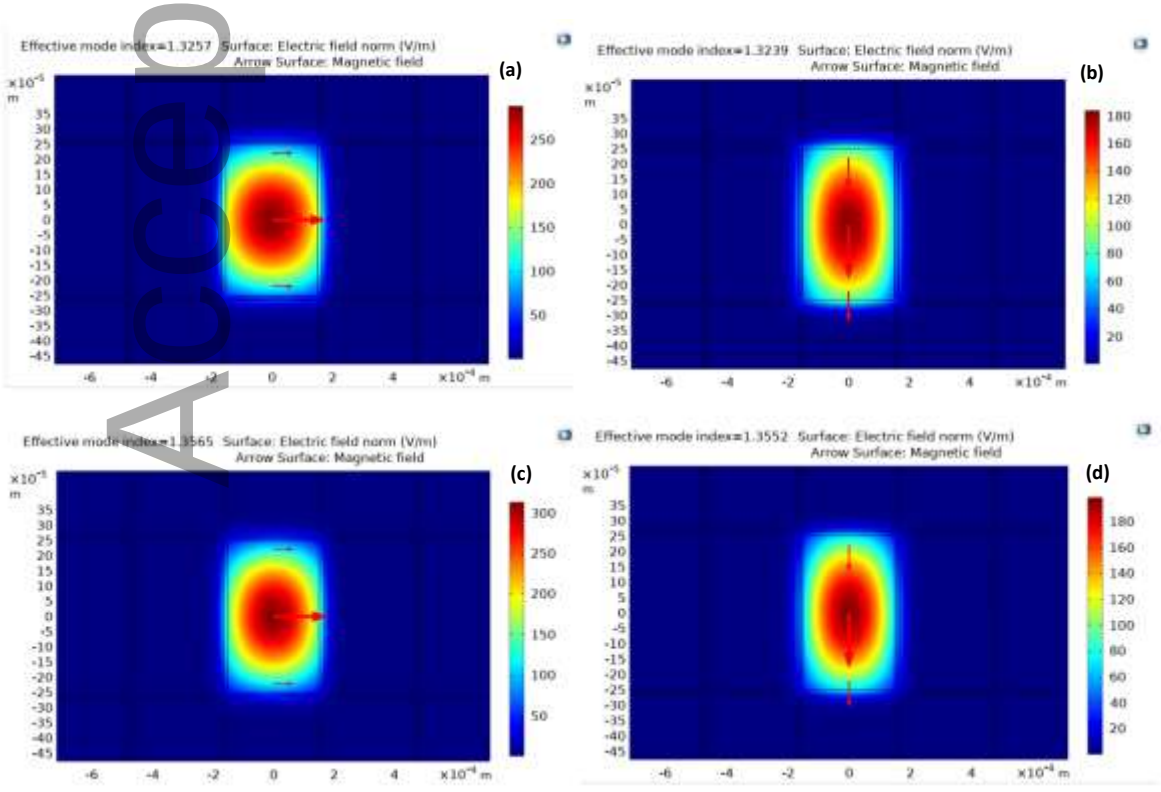

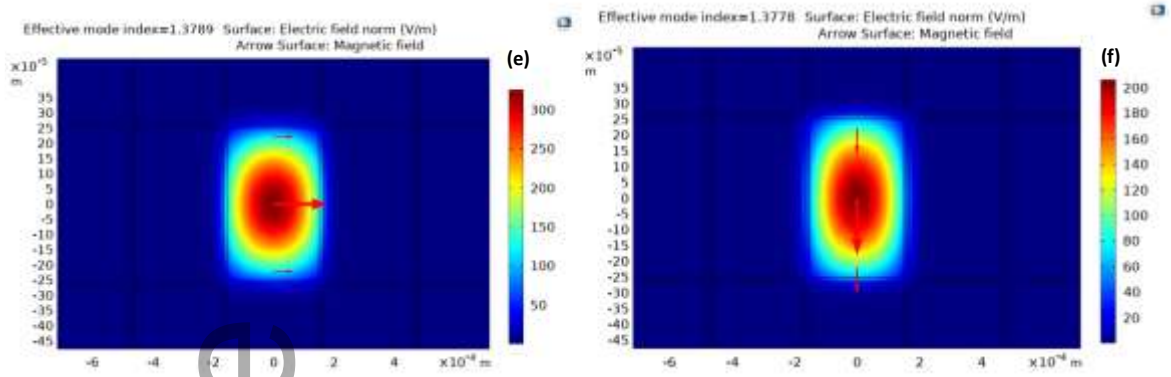

Fig. 2. Light propagation of the proposed PCF at a frequency of 2.8 THz, for x-polarized (Figs. 2a, 2c and 2e) and y-polarized (Figs. 2b, 2d and 2f) for pure water (Figs. 2a and 2b), V. Cholera (Figs. 2c and 2d) and E. Coli (Figs. 2e and 2f).

3. Mathematical analysis of the model

For the purpose of numerical simulation, we have employed COMSOL Multiphysics version 5.6 which is based on the finite element method. We have divided the investigation into three circumstances: optimal +2%, optimal, and optimal -2%. In the two cases of optimal ±2, the core width is changed by ±2% to create these conditions. The core's width and height are chosen at 300 μm and 500 μm, respectively, for the optimum case. The width of the core is chosen at 306 μm and 294 μm for the cases of optimum +2% and -2%, respectively. The analyte is first inserted into the PCF core in order to start the analysis. The RI of a material determines the speed of light while it is traveling through it. Based on particular sensing properties, such as relative sensitivity, confinement loss, power ratio, effective area and birefringence, the sensor performance can be evaluated.

The definitions for these terms can be summarized as follows. Relative sensitivity of a PCF refers to the change in a PCF's optical properties (e.g., wavelength, intensity) due to a change in an external parameter (e.g., temperature, pressure, refractive index). It quantifies how responsive the PCF is to changes in the parameters it is designed to sense. Confinement loss of a PCF is the loss of light energy due to the finite guidance of optical modes within the core of the fiber. It occurs when light leaks out of the core and into the cladding or surrounding medium. Minimizing confinement loss is important for efficient light transmission. The power ratio of a PCF typically refers to the ratio of optical power carried by the fundamental mode (the mode with the highest intensity in the core) to the total optical power within the fiber. It indicates how much of the light is concentrated in the core mode, which affects the fiber's performance. The effective area of a PCF is a measure of the spatial extent of an optical mode within the fiber core. It quantifies how tightly or loosely the optical mode is confined. A larger effective area implies a more extended mode, which can be advantageous for certain applications like high-power laser delivery. Birefringence of a PCF refers to the difference in refractive indices for light polarized in different directions within the fiber. PCF can exhibit birefringence due to its structural asymmetry. Controlling birefringence can be important for polarization-sensitive applications.

The most essential property is relative sensitivity as it shows in what amount of an analyte holds the specific sensing elements. Usually, sensing is performed by matching the RI. Calculating light intensity that directly interacts with the sensor analyte is necessary to determine the relative sensitivity. The relative sensitivity significantly depends upon the power ratio (PF) which is used for measuring the light extent associated with the analytes in the core. It is given by [11]

$$PF = \frac{\int_{analyte} Re\{E_x H_y - H_x E_y\} dxdy}{\int_{total} Re\{E_x H_y - H_x E_y\} dxdy}, \% \quad (1)$$

The numerator and denominator, respectively, give the amount of light propagating in the core and total cross-sectional areas. When n_r and n_{eff} are the RIs of the analyte and the effective modal RI, the relative sensitivity (*RS*) to an analyte is calculated using the following Eq. [12]

$$RS = \frac{n_r}{n_{eff}} PF, \% \quad (2)$$

Confinement loss (CL) is defined as the loss which takes place when the optical confinement decreases as a result of the PCF's cladding-core configuration. This loss is indicated by the amount of light that is captured by the air holes of the cladding area. The sensor quality will be better when the CL is lower. When $k_0 = 2\pi / \lambda$, λ is the light wavelength. The CL is given by [13]

$$CL = 8.686 \times k_0 \times Imginary(n_{eff}) \times 10^{-2}, cm^{-1} \quad (3)$$

where $Imginary(n_{eff})$ gives the imaginary part of the modal RI.

The asymmetry between the organization of the cladding and the core regions is known as birefringence. It is considered an optical property of the fiber material. Light propagation and polarization can affect the birefringence. If the RIs of the fiber in the x and y polarization directions are described by n_{eff}^x and n_{eff}^y, the birefringence is given by [14]

$$Birefringence = \left|Re\{n_{eff}^x - n_{eff}^y\}\right| \quad (4)$$

Depending on the electric field, light can occasionally propagate out from the analyte in the core region. The effective area (*EA*) is the region where analyte sensing is most efficient. A lower *EA* with a substantial nonlinear effect can produce a high-power density in the zone. The *EA*, sometimes indicated as A_{eff}, can be written as [11]

$$A_{\text{eff}} = \frac{(\int |E^2| dxdy)^2}{\int |E^4| dxdy}, \mu m^2 \quad (5)$$

The background substance can add a significant amount of loss which is called effective material loss (EML) which can be reduced by reducing the amount of background substance. To calculate the EML, the following equation can be used [13]

$$EML = \frac{\sqrt{\frac{\varepsilon_0}{\mu_0}} \int_{mat} \eta_{mat} \alpha_{mat} |E|^2 dA}{\left| \int_{all} \frac{1}{2} (E \times H^*) z dA \right|}, cm^{-1} \quad (6)$$

where, η_{mat} and α_{mat} stand for the RI and bulk absorption parameter (cm^{-1}) for the material fiber (Zeonex), respectively, $\eta_{Zeonex} = 1.53$, and $\alpha_{Zeonex} = 0.2\ cm^{-1}$. E and H^* denote the electric and transverse magnetic signals, respectively. The μ_0 and ε_0 symbolize the permeability and permittivity of free space. All the parameters that have been used in the simulation are reported in Table 1.

The largest acceptable angle of incidence of injected light is known as the numerical aperture (*NA*). Operation frequency (*f*), light speed (*c*), and *EA* all affect the *NA* value. Since it measures how well a fiber can confine light, a greater value for it is anticipated. It is numerically estimated using Eq. (7) [12]

$$NA = (1 + \pi f^2 A_{\text{eff}} / c^2)^{-1/2} \quad (7)$$

Table 1. The parameters used for the PCF.

The radius of PCF (R)	1650 μm
PML	132 μm
Pitch (p)	15 μm
$w_{cladding}$	300 μm
$h_{cladding}$	500 μm
w_{core} (optimum)	300 μm
h_{core} (optimum)	500 μm
w_{core} (optimum -2%)	294 μm
h_{core} (optimum -2%)	500 μm
w_{core} (optimum +2%)	306 μm
h_{core} (optimum +2%)	500 μm
η_{Zeonex}	1.53
α_{Zeonex}	0.2 cm^{-1}
n_{water}	1.333
$n_{V.Cholera}$	1.365
$n_{E.Coli}$	1.388

4. Simulation results and discussion

For measuring the efficiency of the designed PCF sensor, a number of optical properties (birefringence, effective area, numerical aperture, effective material loss, confinement loss, power factor, and relative sensitivity) should be investigated in the spectral region under consideration (1.5 - 3 THz). The main aim of the current work is the detection of three primary analytes (water, V. Cholera, and E. Coli bacteria) in both polarization directions (x-polarized and y-polarized). The calculations of the above-mentioned optical properties depend on the effective mode index values. The effective mode index variations for the three analytes are depicted in Fig. 3 for both the polarization directions (x and y) in the frequency range of 1.5 - 3 THz.

Figure 3 shows the effective mode index of water (Fig. 3a and 3b), V. Cholera (Fig. 3c and 3d), and E. Coli (Fig. 3e and 3f) analytes in the x-polarized mode (Figs. 3a, 3c, 3e) and y- polarized mode (Figs. 3b, 3d, 3f). Considering the value of the operating frequency of 2.8 THz, the effective mode index of water, V. Cholera, and E. Coli analytes are 1.3257, 1.3565, and 1.3789 in the x-polarised mode and 1.3239, 1.3552, and 1.3778 in the y-polarized mode for the optimum case. For optimum +2% case, the effective mode index of water, V. Cholera, and E. Coli analytes are 1.3242, 1.3556 and 1.3782 in the x-polarised mode and 1.3233, 1.3547 and 1.3775 in the y- polarized mode, respectively. For optimum -2% case, the effective mode index of water, V. Cholera, and E. Coli analytes are 1.3281, 1.3579, and 1.3799 in the x-polarised mode and 1.3248, 1.3558 and 1.3783 in the y- polarized mode, respectively.

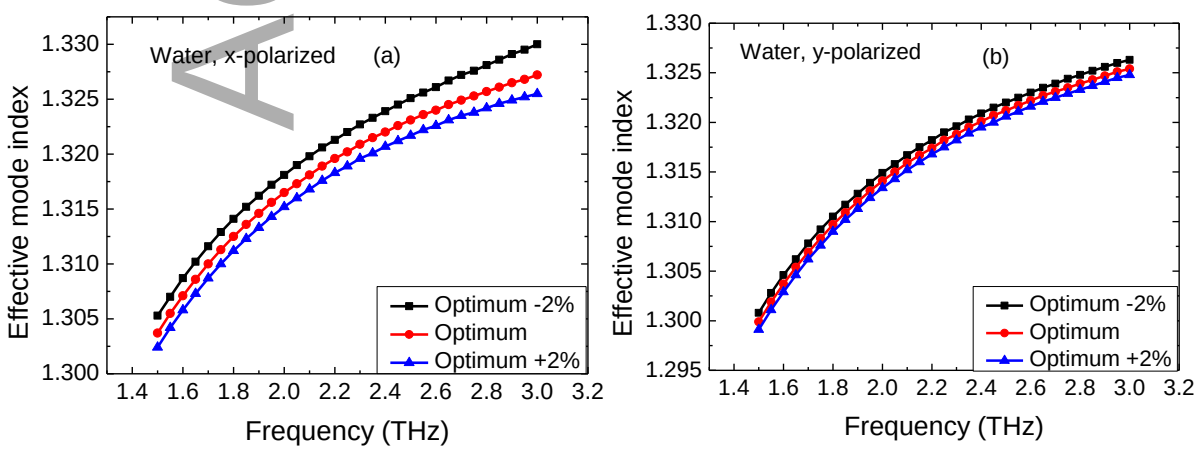

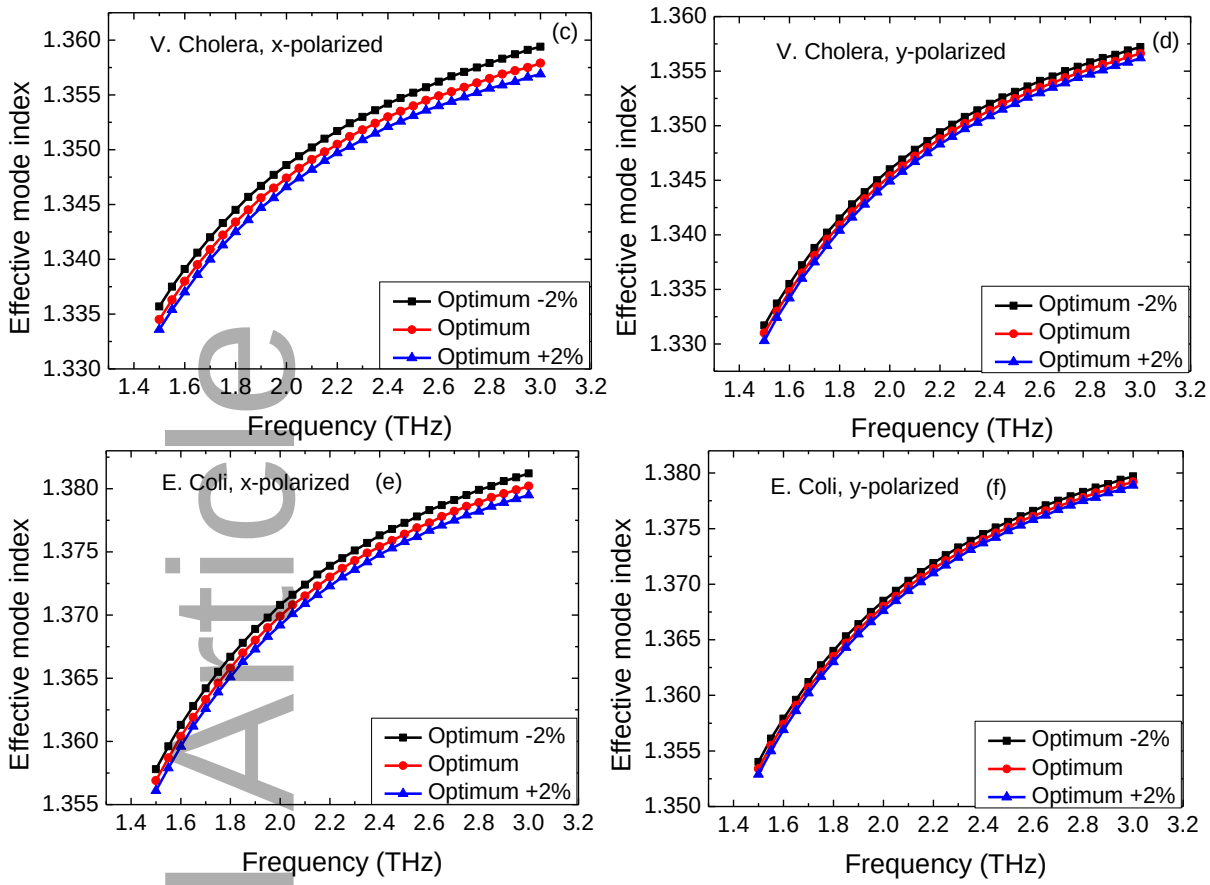

Fig. 3. Effective mode index of pure water (Figs. 3a and 3b), V. Cholera (Figs. 3c and 3d), and E. Coli (Figs. 3e and 3f) analytes for x-polarized mode (Figs. 3a, 3c and 3e) and y-polarized mode (Figs. 3b, 3d and 3f). The three curves in each panel represent optimum -2%, optimum, and optimum +2% structures.

Table 2. reports the effective mode index values at an operating frequency of f = 2.8 THz for the proposed PCF sensor at different structures and polarization. It is clear that the effective mode index values in each case were relatively close to the refractive indices of the analytes. The table also shows as the RI of the analyte increases, the effective mode index increases in all polarizations and PCF geometries.

Table 2: Effective mode index at an operating frequency of f =2.8 THz of the proposed PCF sensor at different analytes, polarizations and PCF structures.

Analyte	Polarizations	PCF structure	Effective mode index (f =2.8 THz)
Water	x-polarization	Optimum -2%	1.3281
		Optimum	1.3257
		Optimum +2%	1.3242
	y-polarization	Optimum -2%	1.3248
		Optimum	1.3239
		Optimum +2%	1.3233
V. Cholera	x-polarization	Optimum -2%	1.3579
		Optimum	1.3565
		Optimum +2%	1.3556
	y-polarization	Optimum -2%	1.3558
		Optimum	1.3552
		Optimum +2%	1.3547

E. Coli	x-polarization	Optimum -2%	1.3799
		Optimum	1.3789
		Optimum +2%	1.3782
	y-polarization	Optimum -2%	1.3783
		Optimum	1.3778
		Optimum +2%	1.3775

Figure 4 shows the birefringence of water, V. Cholera, and E. Coli analytes, respectively. The values of birefringence at an operating frequency of f = 2.8 THz of water, V. Cholera, and E. Coli analytes are 0.0018, 0.0013 and 0.0011, respectively, for optimum structure. For optimum +2% structure, the birefringence of water, V. Cholera, and E. Coli analytes are 0.0009, 0.0009 and 0.0007, respectively. For optimum −2% structure, the birefringence of water, V. Cholera, and E. Coli are, respectively, equal to 0.0033, 0.0021 and 0.0016.

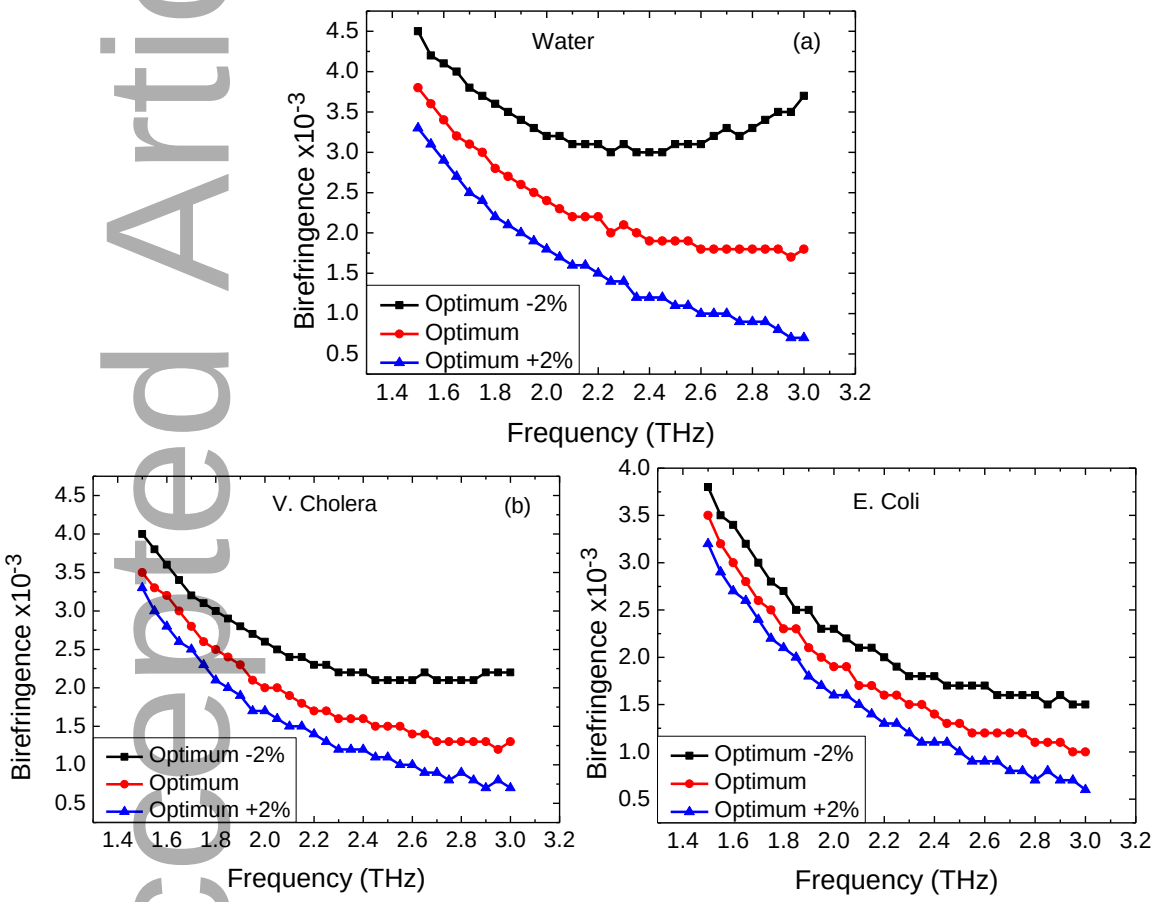

Fig. 4. Birefringence of (a) water, (b) V. Cholera, and (c) E. Coli analytes at an optimum -2%, optimum, and optimum +2% cases.

The values of birefringence at an operating frequency of 2.8 THz for the analytes of water, V. Cholera and E. Coli analytes at different PCF structures are reported in Table 3. Generally, the birefringence of the proposed PCF decreases as the analyte RI increases. Moreover, the structure of -2% optimum has the highest birefringence among all structures. Since higher PCF birefringence is highly praised, optimum -2% structure is recommended for high birefringence.

Table 3: Birefringence values at 2.8 THz, for different sensing analytes at different PCF structures.

Analyte	PCF structure	Maximum birefringence × 10^{-3} (f = 2.8 THz)
Water	Optimum -2%	3.3

	Optimum	1.8
	Optimum +2%	0.9
V. Cholera	Optimum -2%	2.1
	Optimum	1.3
	Optimum +2%	0.9
E. Coli	Optimum -2%	1.6
	Optimum	1.1
	Optimum +2%	0.7

Figure 5 shows the effective area (μm^2) of water (Fig. 5a and 5b), V. Cholera (Fig. 5c and 5d), and E. Coli (Fig. 5e and 5f) analytes in the x-polarized mode (Figs. 5a, 5c, 5e) and y- polarized mode (Figs. 5b, 5d, 5f). At an operating frequency of 2.8 THz, the effective area of water, V. Cholera, and E. Coli analytes are 87761 μm^2, 91955 μm^2 and 93349 μm^2 in the x-polarization and 83635 μm^2, 86985 μm^2 and 88944 μm^2 in the y-polarization for the optimum structure, respectively. For optimum +2% structure, the effective area of water, V. Cholera, and E. Coli analytes are 81290 μm^2, 87270 μm^2 and 89823 μm^2 in the x- polarization and 99811 μm^2, 97474 μm^2, 96314 μm^2 in the y-polarization, respectively. For optimum -2% structure, the effective area of water, V. Cholera, and E. Coli analytes are 96595 μm^2, 98642 μm^2, 98331 μm^2 in the x- polarized mode and 63575 μm^2, 71948 μm^2, 77683 μm^2 in the y-polarized mode, respectively.

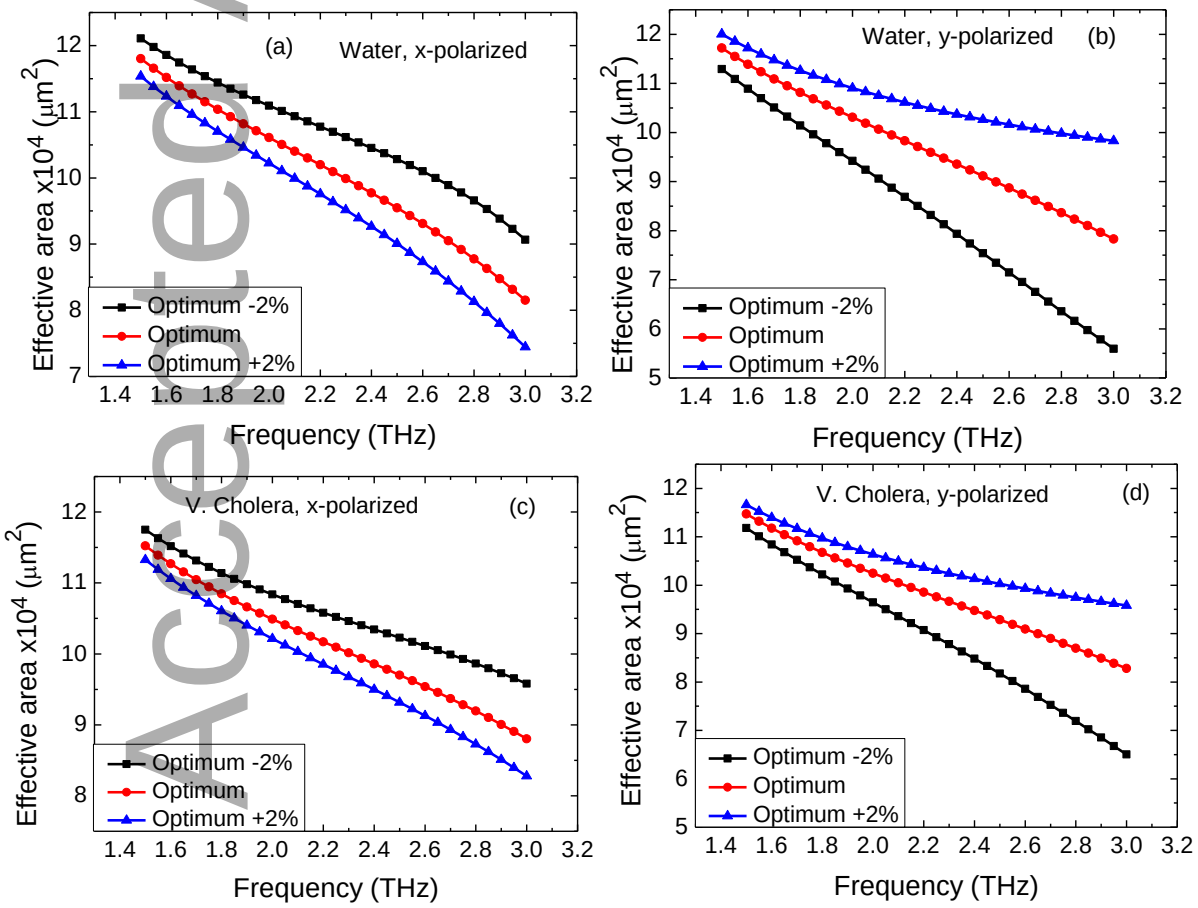

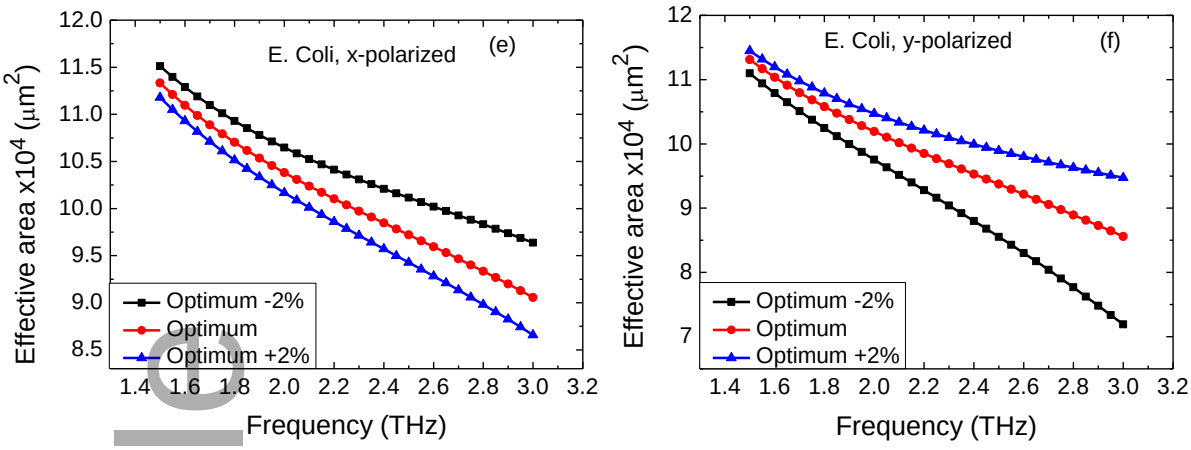

Fig. 5. Effective area (μm^2) for pure water (Figs. 5a and 5b), V. Cholera (Figs. 5c and 5d), and E. Coli (Figs. 5e and 5f) analytes for x-polarized mode (Figs. 5a, 5c and 5e) and y-polarized mode (Figs. 5b, 5d and 5f). The three curves in each panel represent optimum -2%, optimum, and optimum +2% structures.

Table 4 presents the effective area of the proposed PCF sensor at f = 2.8 THz for all the analytes under consideration. Both polarizations and different PCF geometries are reported. For x-polarization, the effective area decreases when the PCF geometry changes from an optimum -2% to the optimum case and then to the optimum +2% case. The y-polarization shows an opposite behavior, the effective area increases when the PCF shape changes from an optimum -2% case to the optimum and then to optimum +2% case, respectively. For an efficient PCF sensor, the effective area should be as low as possible. Thus, the structure of optimum +2% and the structure of optimum -2% are the best choices for x-polarization and y-polarization, respectively.

Table 4: Effective area at f = 2.8 THz of the proposed PCF sensor at different analytes for different PCF structures in x-polarization and y-polarization.

Analyte	Polarizations	PCF structure	$A_{eff} \times 10^4$ (μm^2) (at f=2.8 THz)
Water	x-polarization	Optimum -2%	9.6595
		Optimum	8.7761
		Optimum +2%	8.129
	y-polarization	Optimum -2%	6.3575
		Optimum	8.3635
		Optimum +2%	9.9811
V. Cholera	x-polarization	Optimum -2%	9.8642
		Optimum	9.1955
		Optimum +2%	8.727
	y-polarization	Optimum -2%	7.1948
		Optimum	8.6985
		Optimum +2%	9.7474
E. Coli	x-polarization	Optimum -2%	9.8331
		Optimum	9.3349
		Optimum +2%	8.9823
	y-polarization	Optimum -2%	7.7683
		Optimum	8.8944
		Optimum +2%	9.6314

Figure 6 shows the numerical aperture of water, V. Cholera, and E. Coli analytes in the x-polarized mode (Figs. 6a, 6c and 6e) and y-polarized mode (Figs. 6b, 6d and 6f). The numerical aperture of water, V. Cholera, and E. Coli analytes are 0.19998, 0.19554 and 0.19413, respectively, in the x-polarization and 0.20465, 0.20083 and 0.1987, in the y-polarization for the optimum structure. For the optimum +2% structure, the numerical aperture of water, V. Cholera, and E. Coli analytes are 0.20746, 0.20052 and 0.19776, respectively, in the x-polarization and 0.18797, 0.19013 and 0.19123, in the y-polarization. For the optimum -2% structure, the numerical aperture of water, V. Cholera, and E. Coli analytes are 0.19097, 0.18904 and 0.18933, respectively, in the x-polarized and 0.23319, 0.2199 and 0.21201, in the y-polarized.

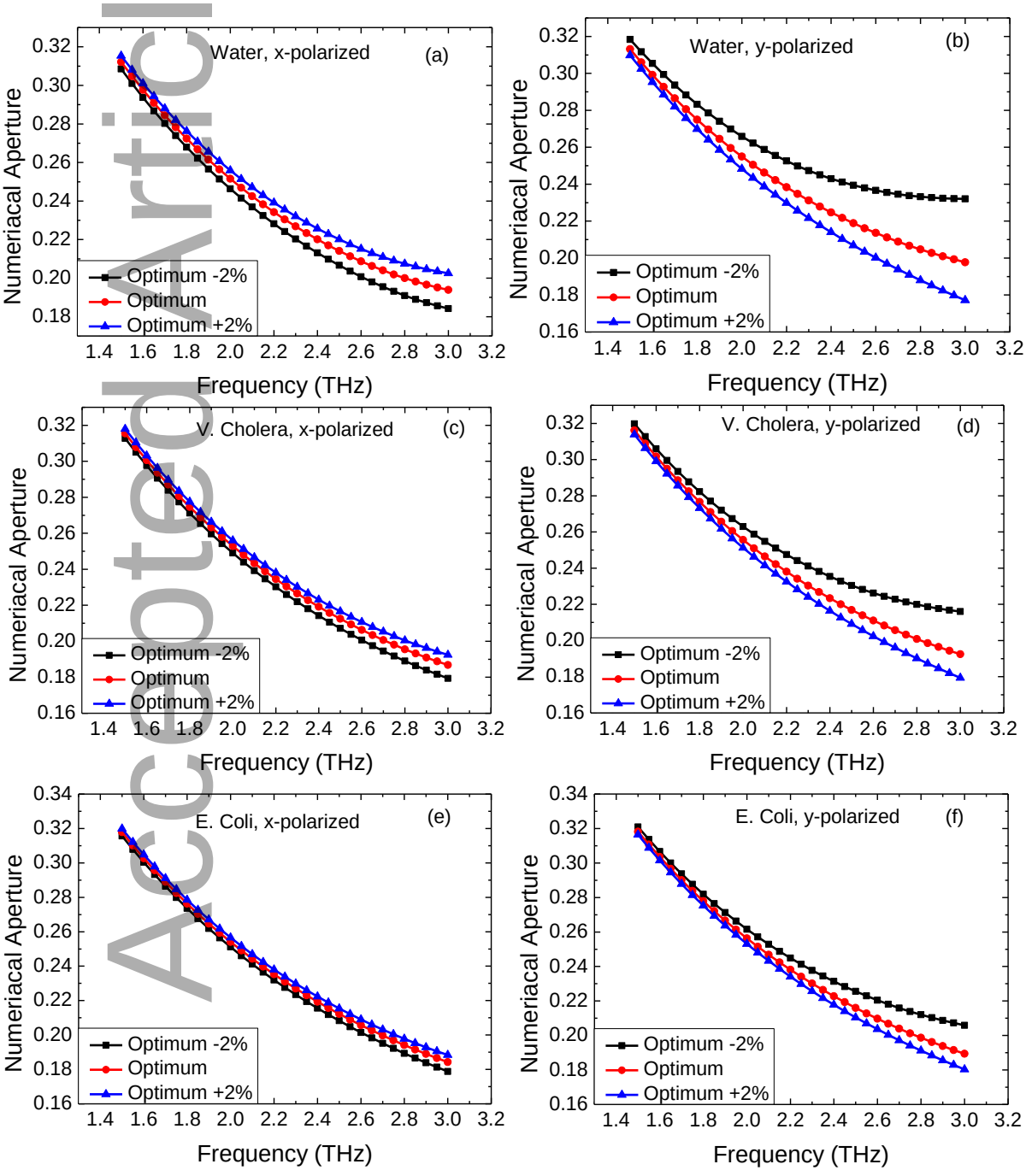

Fig. 6. Numerical aperture for pure water (Figs. 6a and 6b), V. Cholera (Figs. 6c and 6d), and E. Coli (Figs. 6e and 6f) analytes for x-polarized mode (Figs. 6a, 6c and 6e) and y-polarized mode (Figs. 6b,

6d and 6f). The three curves in each panel represent optimum -2%, optimum, and optimum +2% structures.

Table 5 reports the numerical aperture at an operating frequency of 2.8 THz for different PCF sensor structures at both polarizations. The maximum values of the numerical aperture at x-polarization are found in the optimum +2% structure. On the other hand, for y-polarization, the optimum -2% structure has the highest values of numerical aperture. Therefore, the best choices for the numerical aperture to be as high as possible are optimum +2% and optimum -2%, for x- and y-polarizations, respectively.

Table 5: The values of numerical aperture at 2.8 THz of the proposed PCF sensor at different analytes for different PCF structures in x-polarization and y-polarization.

Analyte	Polarizations	PCF structure	NA (at f=2.8 THz)
Water	x-polarization	Optimum -2%	0.19097
		Optimum	0.19998
		Optimum +2%	0.20746
	y-polarization	Optimum -2%	0.23319
		Optimum	0.20465
		Optimum +2%	0.18797
V. Cholera	x-polarization	Optimum -2%	0.18904
		Optimum	0.19554
		Optimum +2%	0.20052
	y-polarization	Optimum -2%	0.2199
		Optimum	0.20083
		Optimum +2%	0.19013
E. Coli	x-polarization	Optimum -2%	0.18933
		Optimum	0.19413
		Optimum +2%	0.19776
	y-polarization	Optimum -2%	0.21201
		Optimum	0.1987
		Optimum +2%	0.19123

Figure 7 illustrates the effective material loss of water, V. Cholera, and E. Coli analytes in the x-polarized mode (Figs. 7a, 7c and 7e) and y-polarized mode (Figs. 7b, 7d and 7f). The effective material loss of water, V. Cholera, and E. Coli analytes are 0.0162, 0.0111 and 0.00869 cm^{-1} in the x-polarization and 0.00831, 0.00537 and 0.00414 cm^{-1} in the y-polarization for the optimum structure, respectively. For optimum +2% structure, the effective material loss of water, V. Cholera, and E. Coli analytes are found as 0.00846, 0.00626 and 0.00514 cm^{-1} in the x-polarization and 0.00727, 0.00452 and 0.0034 cm^{-1} in the y-polarization, respectively. For optimum -2% structure, the effective material loss of water, V. Cholera, and E. Coli bacteria are 0.03093, 0.01958, and 0.01454 cm^{-1} in the x-polarization and 0.01013, 0.00676, and 0.00536 cm^{-1} in the y-polarization, respectively. All the above-mentioned values of the effective material loss are evaluated at f = 2.8 THz. The effective material loss has to be as low as possible. The best structure that has the lowest effective material loss is the optimum +2% structure.

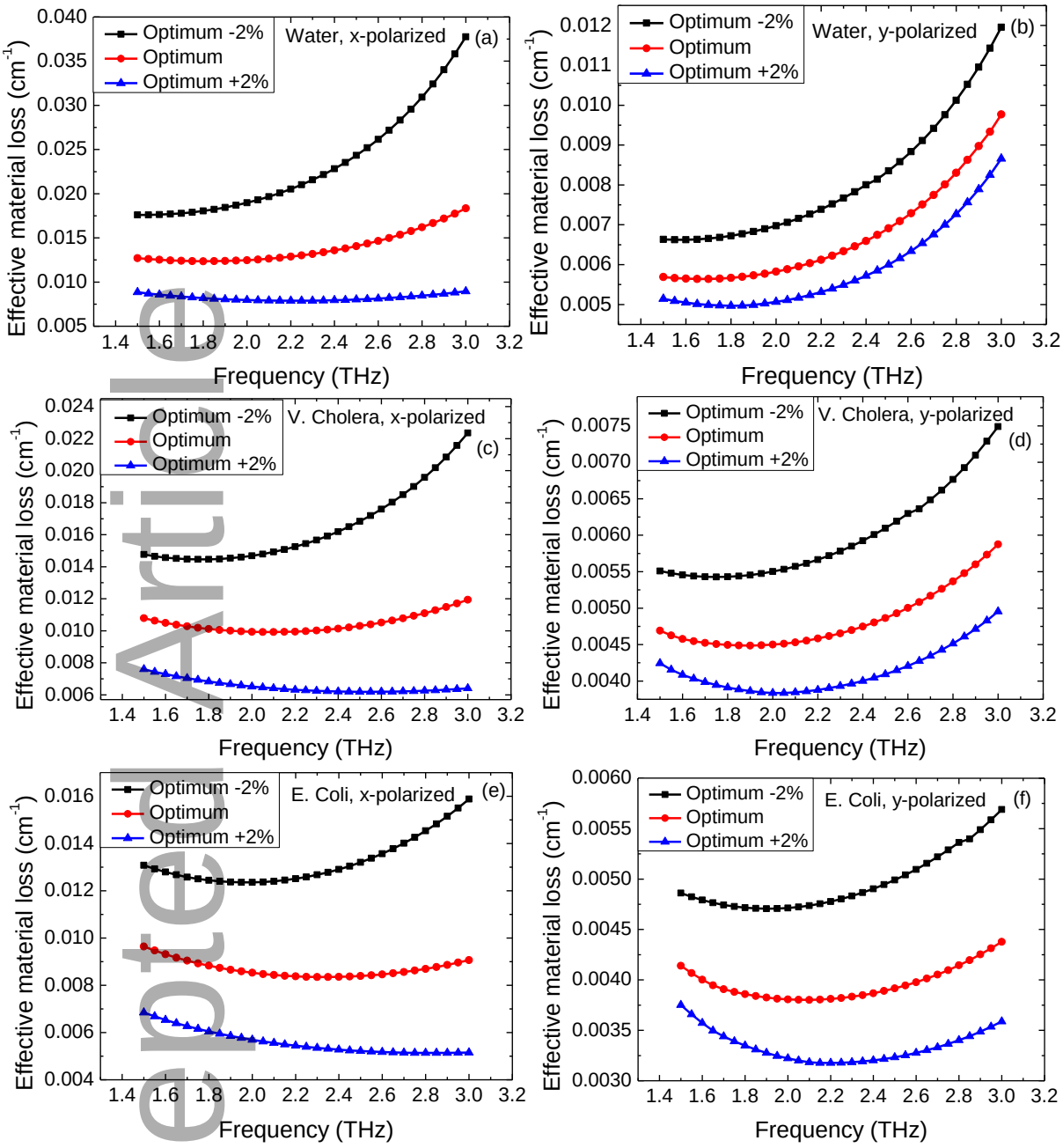

Fig. 7. Effective material loss for pure water (Figs. 7a and 7b), V. Cholera (Figs. 7c and 7d), and E. Coli (Figs. 7e and 7f) analytes for x-polarized mode (Figs. 7a, 7c and 7e) and y-polarized mode (Figs. 7b, 7d and 7f). The three curves in each panel represent optimum -2%, optimum, and optimum +2% structures.

Table 6 shows the values of effective material loss for water, V. Cholera and E. Coli PCF sensors at f = 2.8 THz, and at optimum -2%, optimum, and optimum +2% structures. Both polarizations (x and y) are considered. As the RI of the analyte increases, the effective material loss decreases for all structures. It is also observed that x-polarization for all PCF sensors has effective material loss values greater than those of y-polarization.

Table 6: Effective material loss at a frequency of 2.8 THz of the proposed PCF sensor, at different analytes for different PCF structures in x- and y-polarizations.

Analyte	Polarizations	PCF structure	*EML* (at f=2.8 THz)

Water	x-polarization	Optimum -2%	0.03093
		Optimum	0.0162
		Optimum +2%	0.00846
	y-polarization	Optimum -2%	0.01013
		Optimum	0.00831
		Optimum +2%	0.00727
V. Cholera	x-polarization	Optimum -2%	0.01958
		Optimum	0.0111
		Optimum +2%	0.00626
	y-polarization	Optimum -2%	0.00676
		Optimum	0.00537
		Optimum +2%	0.00452
E. Coli	x-polarization	Optimum -2%	0.01454
		Optimum	0.00869
		Optimum +2%	0.00514
	y-polarization	Optimum -2%	0.00536
		Optimum	0.00414
		Optimum +2%	0.0034

Figure 8 shows the confinement loss of water (Fig. 8a and 8b), V. Cholera (Fig. 8c and 8d), and E. Coli (Fig. 8e and 8f) analytes in the x-polarized mode (Figs. 8a, 8c, 8e) and y- polarized mode (Figs. 8b, 8d, 8f). At an operating frequency of 2.8 THz, the confinement loss of water, V. Cholera, and E. Coli analytes are 0.60245×10^{-14}, 0.86591×10^{-14} and 2.0814×10^{-14} cm^{-1} in the x-polarized mode and 0.77872×10^{-14}, 1.6493×10^{-14}, and 4.0028×10^{-14} cm^{-1} in the y-polarized mode for the optimum structure. The confinement loss of water, V. Cholera, and E. Coli analytes are 0.87677×10^{-14}, 0.1×10^{-14}, and 0.1×10^{-14} cm^{-1} in the x-polarized mode and 3.0288×10^{-14}, 2.0777×10^{-14}, 5.297×10^{-14} cm^{-1} in the y-polarized mode, respectively, for optimum +2% structure. For optimum -2% structure, the confinement loss of water, V. Cholera, and E. Coli bacteria are 2.0477×10^{-14}, 2.4073×10^{-14} and 3.3256×10^{-14} cm^{-1} in the x-polarization and 1.9347×10^{-14}, 0.24629×10^{-14} and 4.6819×10^{-14} cm^{-1} in the y-polarization, respectively. As can be observed in Fig. 8, the confinement loss oscillates with the variation of the frequency but it is very low for all structures.

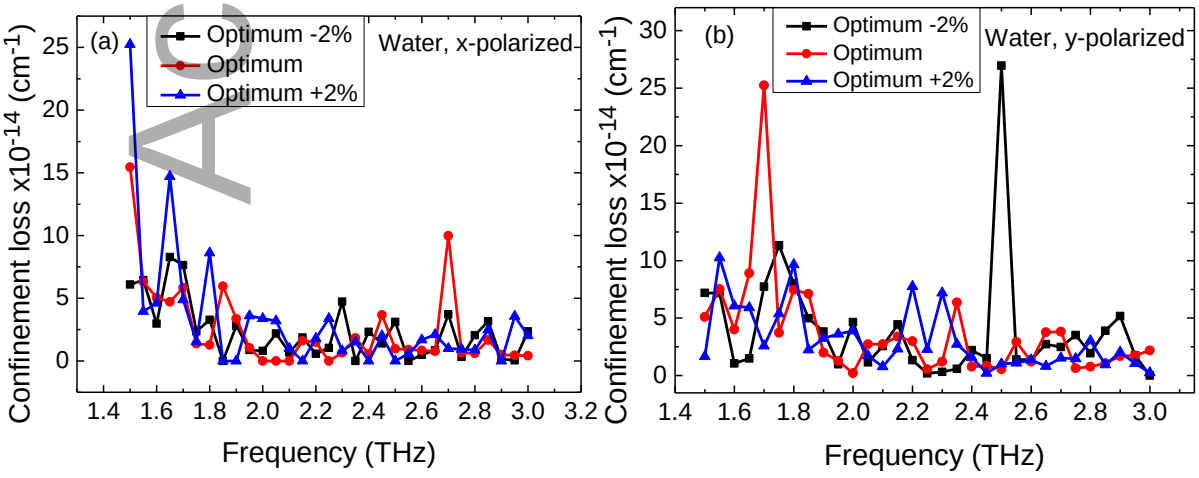

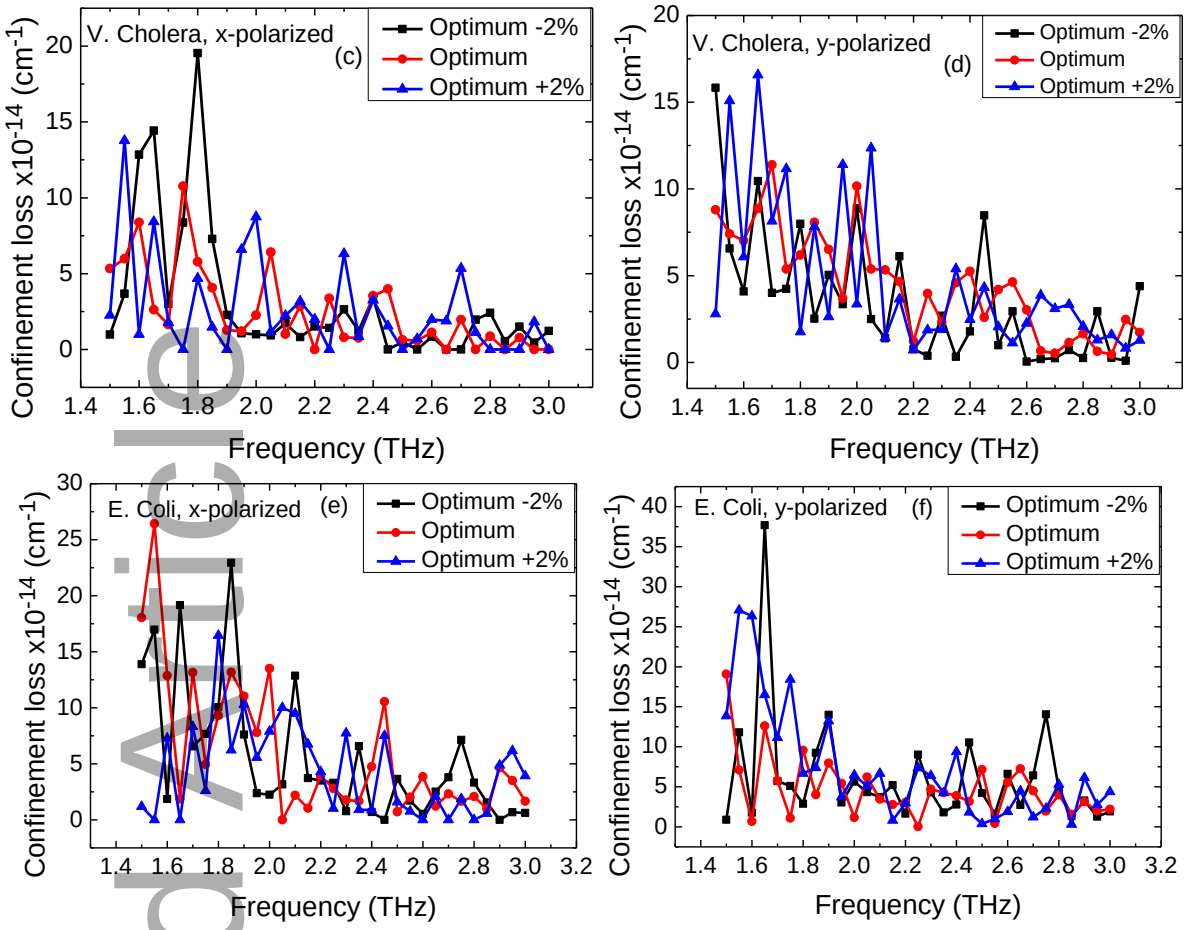

Fig. 8. Confinement loss (cm^{-1}) for pure water (Figs. 8a and 8b), V. Cholera (Figs. 8c and 8d), and E. Coli (Figs. 8e and 8f) analytes for x-polarized mode (Figs. 8a, 8c and 8e) and y-polarized mode (Figs. 8b, 8d and 8f). The three curves in each panel represent optimum -2%, optimum, and optimum +2% structures.

Table 7 shows the confinement loss values at 2.8 THz for different analytes at x- and y-polarizations. As can be seen, the minimum value of the confinement loss is $0.1\times 10^{-14}\ cm^{-1}$ and it happens at optimum +2% structure at x-polarization for V. Cholera and E. Coli PCF sensors.

Table 7: Confinement loss at 2.8THz of the proposed PCF sensor, at different analytes for different PCF structures in x- and y-polarizations.

Analyte	Polarizations	PCF structure	Confinement loss × 10^{-14} (at f = 2.8 THz)
Water	x-polarization	Optimum -2%	2.0477
		Optimum	0.60245
		Optimum +2%	0.87677
	y-polarization	Optimum -2%	1.9347
		Optimum	0.77872
		Optimum +2%	3.0288
V. Cholera	x-polarization	Optimum -2%	2.4073
		Optimum	0.86591
		Optimum +2%	0.1
	y-polarization	Optimum -2%	0.24629

		Optimum	1.6493
		Optimum +2%	2.0777
E. Coli	x-polarization	Optimum -2%	3.3256
		Optimum	2.0814
		Optimum +2%	0.1
	y-polarization	Optimum -2%	4.6819
		Optimum	4.0028
		Optimum +2%	5.297

Figure 9 shows the power factor of water (Fig. 9a and 9b), V. Cholera (Fig. 9c and 9d), and E. Coli (Fig. 9e and 9f) analytes in the x-polarization (Figs. 9a, 9c, 9e) and y- polarization (Figs. 9b, 9d, 9f). At an operating frequency of 2.8 THz, the power factor of water, V. Cholera, and E. Coli bacteria are 90.067%, 93.15% and 94.614% in the x-polarized mode and 93.692%, 95.759% and 96.659% in the y-polarized mode for the optimum structure, respectively. For optimum +2% structure, the power factor of water, V. Cholera, and E. Coli analytes are 94.114%, 95.67% and 96.453% in the x-polarized mode and 94.598%, 96.465%, 97.253% in the y-polarized mode, respectively. For optimum -2% structure, the power factor of water, V. Cholera, and E. Coli analytes are 82.806%, 88.914% and 91.685% in the x-polarized mode and 92.212%, 94.648% and 95.75% in the y-polarized mode, respectively. For an efficient sensor, the power factor should be as high as possible. Therefore, the optimum +2% structure is the best choice since it corresponds to the highest power factor percentages.

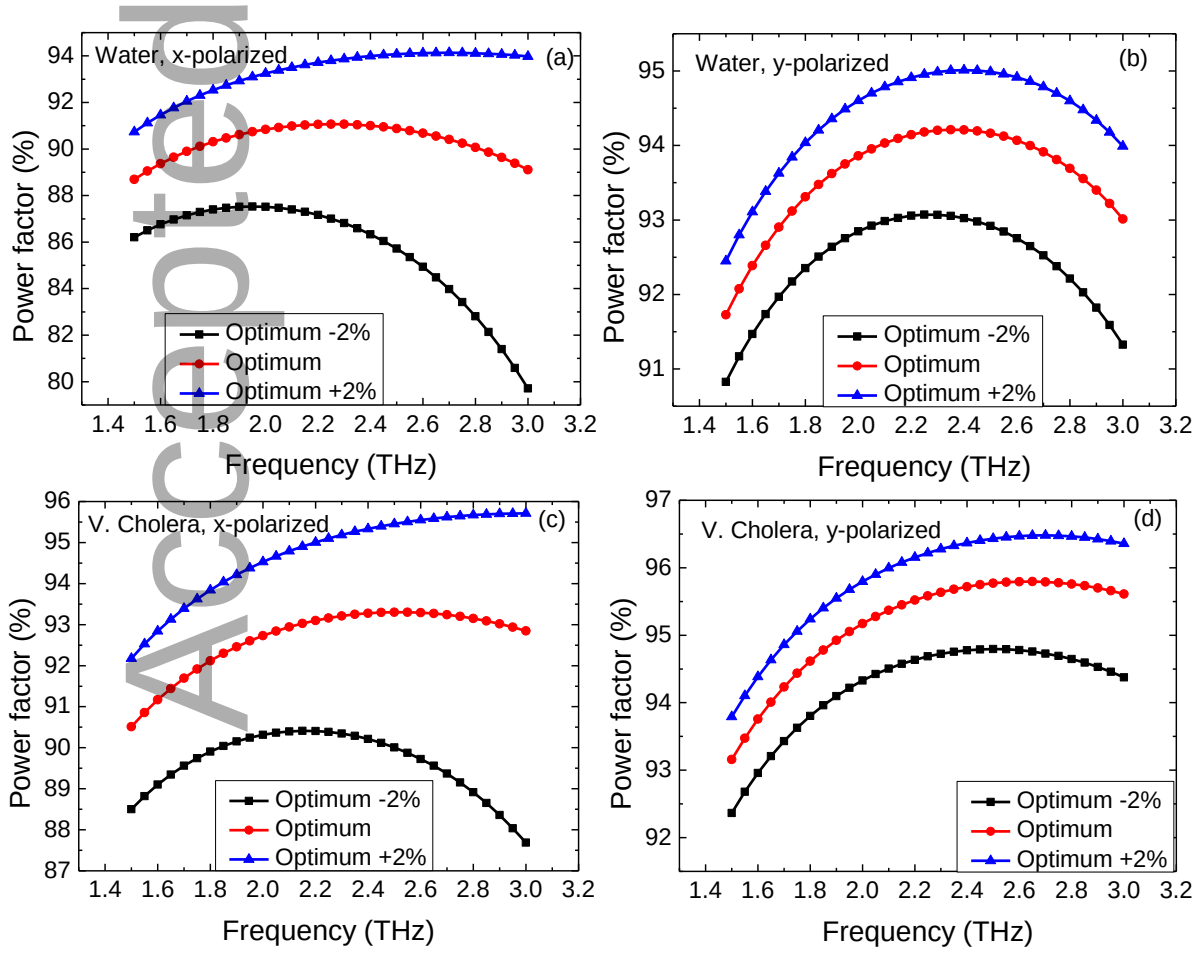

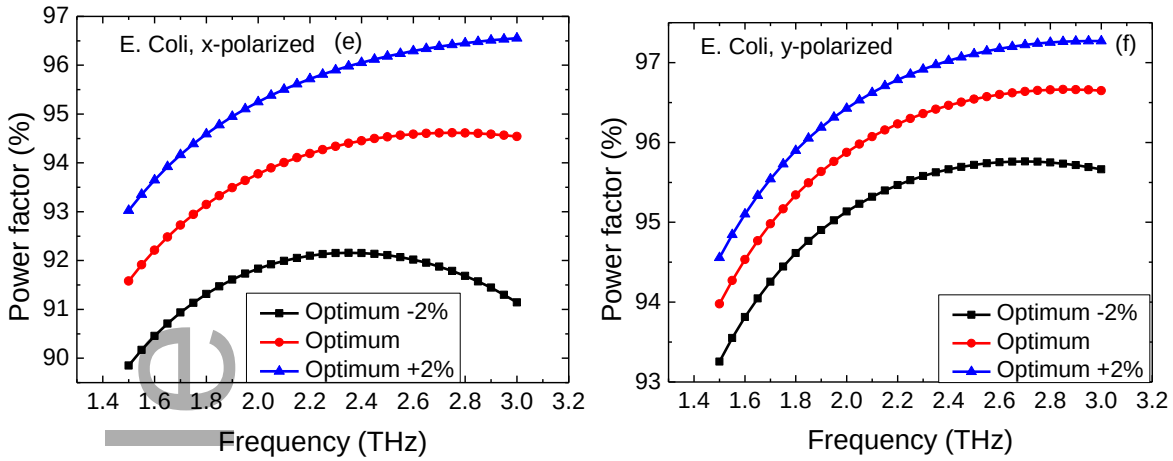

Fig. 9. Power factor (%) for pure water (Figs. 9a and 9b), V. Cholera (Figs. 9c and 9d), and E. Coli (Figs. 9e and 9f) analytes for x-polarized mode (Figs. 9a, 9c and 9e) and y-polarized mode (Figs. 9b, 9d and 9f). The three curves in each panel represent optimum -2%, optimum, and optimum +2% structures.

The power factors at an operating frequency of 2.8 THz for the analytes of water, V. Cholera and E. Coli analytes at different PCF structures are reported in Table 8. As the RI of the analyte increases, the power factor can be enhanced. The y-polarization has higher values of the power factor than the x-polarization.

Table 8: The power factor at 2.8 THz of the proposed PCF sensor, at different analytes for different PCF structures in x- and y-polarizations.

Analyte	Polarizations	PCF structure	*PF* % (at f=2.8 THz)
Water	x-polarization	Optimum -2%	82.806
		Optimum	90.067
		Optimum +2%	94.114
	y-polarization	Optimum -2%	92.212
		Optimum	93.692
		Optimum +2%	94.598
V. Cholera	x-polarization	Optimum -2%	88.914
		Optimum	93.15
		Optimum +2%	95.67
	y-polarization	Optimum -2%	94.648
		Optimum	95.759
		Optimum +2%	96.465
E. Coli	x-polarization	Optimum -2%	91.685
		Optimum	94.614
		Optimum +2%	96.453
	y-polarization	Optimum -2%	95.75
		Optimum	96.659
		Optimum +2%	97.253

Figure 10 depicts the relative sensitivity of water, V. Cholera, and E. Coli analytes in the x-polarized mode (Figs. 10a, 10c and 10e) and y-polarized mode (Figs. 10b, 10d and 10f). The relative sensitivity of water, V. Cholera, and E. Coli analytes are 90.561%, 93.733% and 95.237% in the x-polarized

mode and 94.333%, 96.453% and 97.373% in the y-polarized mode for the optimum structure, respectively. For optimum +2% structure, the relative sensitivity of water, V. Cholera, and E. Coli analytes are 94.739%, 96.335% and 97.135% in the x-polarized mode and 95.288%, 97.195% and 97.996% in the y-polarized mode, respectively. For optimum -2% structure, the relative sensitivity of water, V. Cholera, and E. Coli analytes are 83.11%, 89.378% and 92.225% in the x-polarized mode and 92.784%, 95.29% and 96.425% in the y-polarized mode, respectively. The highest sensitivity of the proposed PCF sensor can be obtained with optimum +2% structure for y-polarized mode due to the high power factor of this structure.

The polarization sensitivity of a PCF sensor refers to how the sensor's response varies with the polarization state of the input light. In other words, it measures how sensitive the sensor's output is to changes in the polarization of the incident light. The designed PCF is considered a polarization-insensitive PCF sensor.

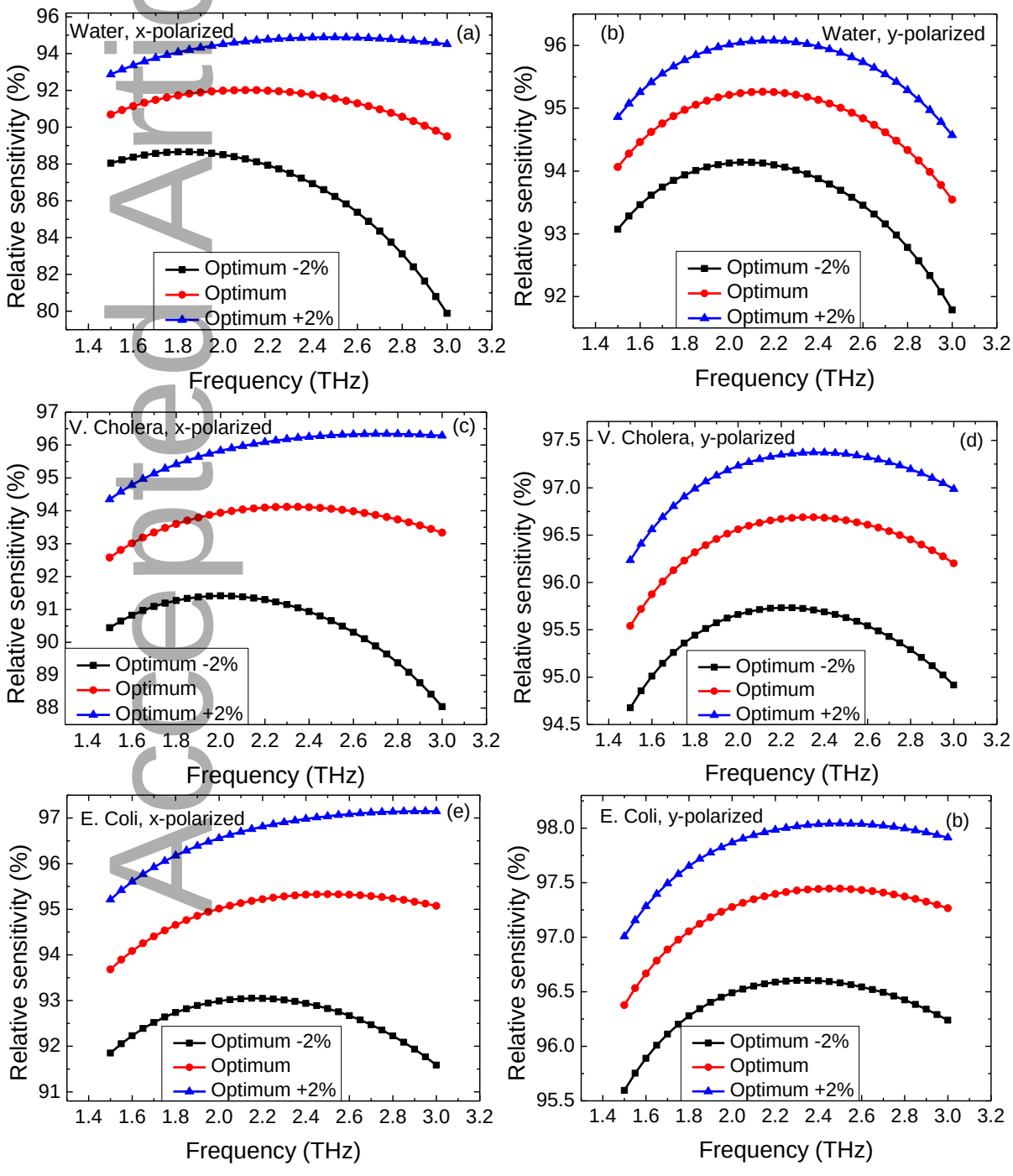

Fig. 10. Relative sensitivity (%) for pure water (Figs. 10a and 10b), V. Cholera (Figs. 10c and 10d), and E. Coli (Figs. 10e and 10f) analytes for x-polarized mode (Figs. 10a, 10c and 10e) and y-polarized mode (Figs. 10b, 10d and 10f). The three curves in each panel represent optimum -2%, optimum, and optimum +2% structures.

It is worth mentioning that altering the size of the rectangular air holes in a PCF sensor can have several effects on its performance and sensing capabilities. Changing the size of the air holes can shift the spectral response of the PCF sensor. Smaller air holes can lead to a blue shift in the resonance wavelength, making the sensor more sensitive to changes in the surrounding medium's refractive index at shorter wavelengths. Reducing the size of the air holes generally increases the sensitivity of the PCF sensor. This means that it becomes more responsive to variations in the refractive index of the surrounding medium, making it suitable for detecting even smaller changes in analyte concentration. Smaller air holes can lead to increased confinement of light within the core, reducing confinement loss. Lower confinement loss can result in longer light-analyte interaction lengths, improving the overall sensitivity of the sensor. Altering the air hole size affects the effective area of the core mode. Smaller air holes reduce the effective area, leading to stronger light-matter interactions. This enhances the sensitivity but may also increase the risk of higher optical losses due to interactions with contaminants.

Table 9 presents the relative sensitivity at a frequency of 2.8 THz for different PCF structures and polarizations. As the RI of the analyte increases, the relative sensitivity can be considerably improved. When y-polarization is applied, the resulting relative sensitivity is observed to be higher than that corresponding to x-polarization. The relative sensitivity of the proposed PCF sensors is extremely high. The PCF sensor is promising and can be used in bio and chemical sensing.

Tables 2-9 report the optical characteristics of the proposed PCF along with its two variants. These tables demonstrate that a small change in the model structure during fabrication will not result in a significant change in the optical parameters.

Table 9: Relative sensitivity at 2.8 THz of the proposed PCF sensor, at different analytes for different PCF structures in x- and y-polarization.

Analyte	Polarizations	PCF structure	*RS* % (at f=2.8 THz)
Water	x-polarization	Optimum -2%	83.11
		Optimum	90.561
		Optimum +2%	94.739
	y-polarization	Optimum -2%	92.784
		Optimum	94.333
		Optimum +2%	95.288
V. Cholera	x-polarization	Optimum -2%	89.378
		Optimum	93.733
		Optimum +2%	96.335
	y-polarization	Optimum -2%	95.29
		Optimum	96.453
		Optimum +2%	97.195
E. Coli	x-polarization	Optimum -2%	92.225
		Optimum	95.237
		Optimum +2%	97.135
	y-polarization	Optimum -2%	96.425
		Optimum	97.373
		Optimum +2%	97.996

It is significant to demonstrate the difference in sensing performance when rectangular air holes are replaced by circular or elliptical ones. Figure 11 shows a cross-sectional illustration of the elliptical (Fig. 11a) and circular (Fig. 11b) PCFs, where the yellow rectangle represents the core region in which the analyte is injected for sensing purposes. We have considered that the number of air holes is the same in the three PCF configurations. Moreover, all holes (rectangular, circular and elliptical) have the same area. Figure 12 shows the light propagation through these PCFs in the x and y directions. The black-red area shows the maximum light confinement. As can be seen the circular-hole PCF has the least confinement in the core layer. Figure 13 shows the relative sensitivity of the different types of PCF (rectangular, elliptical and circular) for V. Cholera. The relative sensitivities are 93.733%, 45.531% and 10.817% in the x-polarized mode for rectangular, elliptical and circular configurations, resprctively, and they are given by 96.453%, 30.72% and 10.81% in the y-polarized mode for rectangular, elliptical and circular configurations, resprctively. The highest sensitivity was obtained with the rectangular hole configuration. The higher sensitivity of the rectangular hole configuration can be attributed to its ability to provide strong confinement and allow for dispersion engineering.

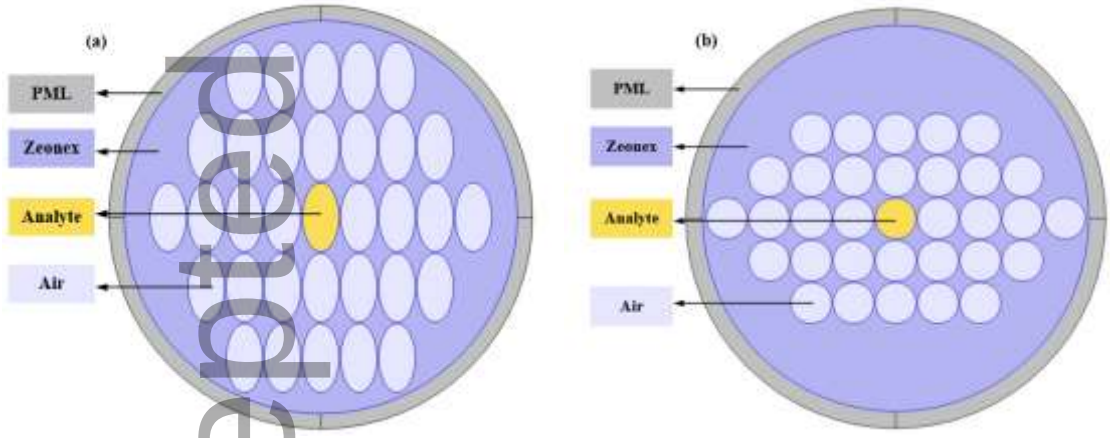

Figure 11. Cross-sectional representation of the proposed (a) elliptical PCF and (b) circular PCF.

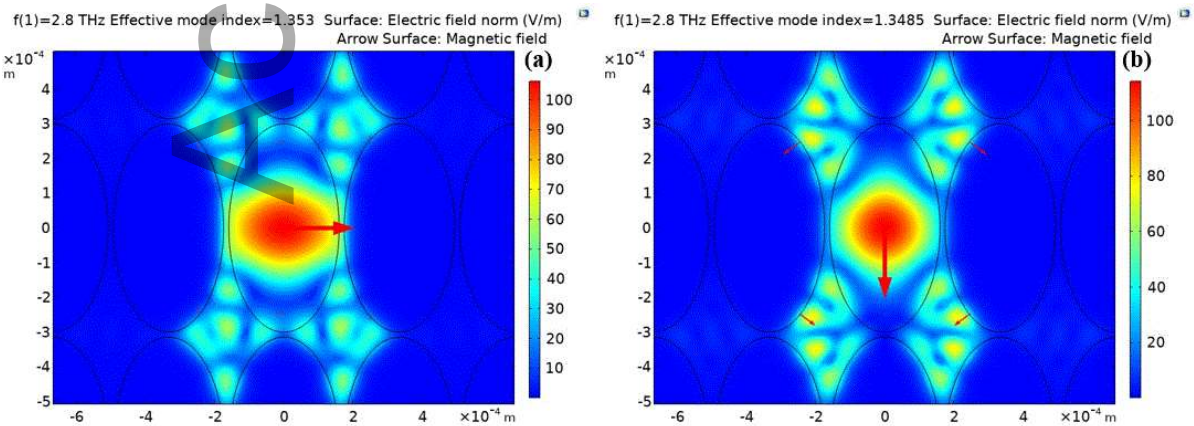

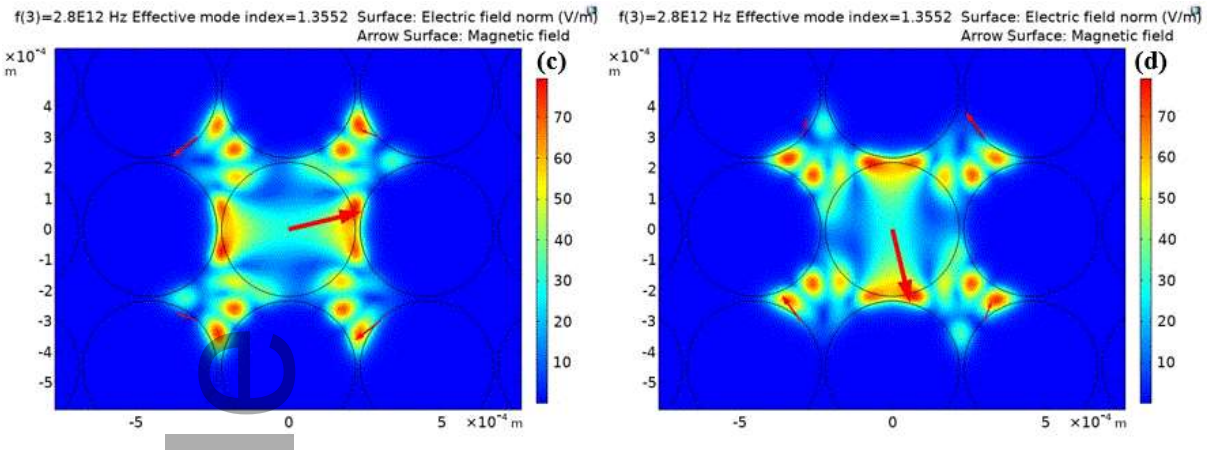

Figure 12. Light propagation of the proposed PCF at a frequency of 2.8 THz, for x-polarized (Figs. 12a and 12c) and y-polarized (Figs. 12b and 12d) for V. Cholera for PCF with elliptical holes (Figs. 12a and b) and PCF with circular holes (Figs. 12c and 12d).

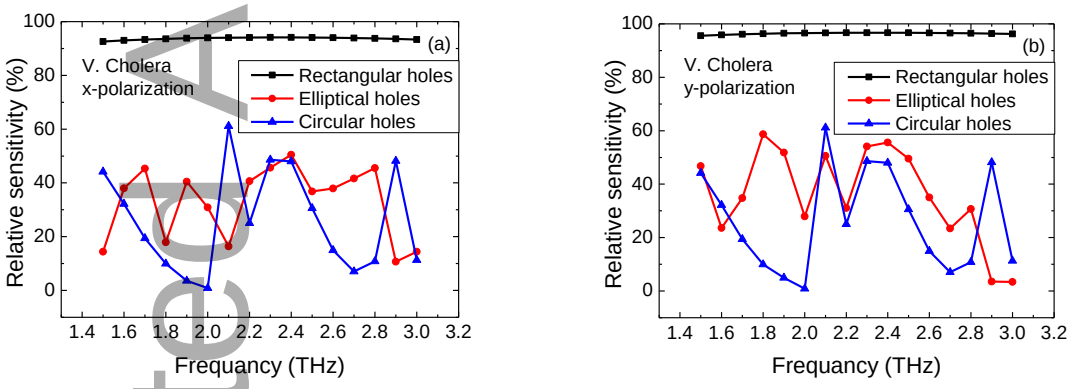

Figure 13. Relative sensitivity (%) for V. Cholera analyte for x-polarized mode (Fig. a) and y-polarized mode (Fig. b). The three curves in each panel represent (black) PCF with rectangular holes, (red) PCF with elliptical holes and (blue) PCF with circular holes.

Table 10: Relative sensitivity at 2.8 THz of the proposed PCF sensors, at different shapes of the PCF holes for V. Cholera in x- and y-polarizations.

PCF hole	Polarizations	*RS* % (at f=2.8 THz)
Rectangular holes	x-polarization	93.733
	y-polarization	96.453
Elliptical holes	x-polarization	45.531
	y-polarization	30.72
Circular holes	x-polarization	10.817
	y-polarization	10.81

Table 11 compares the proposed PCF sensor with the most recently published PCF sensors. As can be seen, the proposed sensor has exceptional efficiency in biosensing.

Table 11: Performance comparison between current work and most recent published PCFs.

Reference	Sensitivity (%)	Confinement loss (cm^{-1})	EML (cm^{-1})	Effective area (μm^2)	Numerical aperture	Birefringence
[16]	41.4	2.17×10^{-12}	-	-	-	0.00509
[17]	49.1	5.58×10^{-7}	-	-	-	0.008
[18]	63.2	2.50×10^{-7}	-	144000	-	-
[19]	91.5	4.87×10^{-11}	0.004	397340	-	-
[20]	90 ± 1	$10^{-16\pm 1}$	0.02	5×10^{4}	-	-
[21]	92.3	5.94×10^{-15}	0.006	209930	-	0.001
[36]	92.2	6.52×10^{-14}	0.0117	93754	0.194	0.001
[40]	94.2	1.28×10^{-13}	0.0059	3.13×10^{5}	0.17707	-
[41]	96.50	2.68×10^{-13}	0.008	1.59×10^{5}	0.225	-
[42]	77.14	2.26×10^{-5}	-	-	-	-
[43]	44.45	6.54×10^{-6}	-	-	-	0.0027
[44]	68.48	2.13×10^{-11}	-	-	-	-
The proposed PCF	97.996	5.297×10^{-14}	0.0034	9.63×10^{4}	0.19123	0.7×10^{-3}

Conclusions

A PCF has been designed and analyzed for detecting V. Cholera and E. Coli bacteria in water. The PCF core consists of a single rectangle and the cladding region has 32 rectangular air holes that have the same dimensions as the core rectangle. Zeonex is employed as the fiber material. Three different structures have been studied and the essential optical parameters have been analyzed for each structure. The operating frequency of the PCF is chosen 2.8 THz. The highest power factor and sensitivity of the proposed PCF sensor have been obtained with optimum +2% structure for y-polarized mode. Many interesting results have been obtained regarding the performance indicators. The effective mode index values in all structures are very close to the refractive indices of the analytes which is a good sign and a birefringence of 3.3×10^{-3} has been obtained. In y-polarization, the following values have been obtained: 97.996% (RS), 6.3575×10^{4} μm^2 (EA), 0.23319 (NA), 0.0034 cm^{-1} (EML), and 0.24629×10^{-14} (CL) have been obtained. In x-polarization, the following values have been obtained: 97.135% (RS), 8.129×10^{4} μm^2 (EA), 0.20746 (NA), 0.00514 cm^{-1} (EML), and 0.1×10^{-14} (CL) have been obtained. These values indicate an efficient PCF sensor. It has been observed that y-polarization has a preference over the x-polarization since it has higher relative sensitivity and numerical aperture. It also has lower effective material loss and effective area compared to x-polarization. The values obtained for the optical parameters demonstrate that a small change in the model structure during fabrication will not result in a significant change in the optical parameters. Moreover, the simplicity of the PCF design ensures the fabrication possibilities of the proposed sensor.

Acknowledgement:
The authors are thankful to the Deanship of Scientific Research at Najran University for funding this work under the Research Groups Funding program grant code (NU/RG/SERC/12/4).

Conflict of Interest: The authors declare that they have no conflict of interest.

Author Contribution:
The authors confirm their contribution to the paper as follows: study conception and design (Dana N. Alhamss, Sofyan A. Taya). Software (Abdulkarem H. M. Almawgani). Interpretation of results (Anurag Upadhyay, Shivam Singh, Ilhami Colak). Draft manuscript preparation (Amrindra Pal, Shobhit K. Patel). Writing the final version (Sofyan A. Taya, Ayman Taher Hindi). Supervision (Sofyan A. Taya). All authors reviewed the results and approved the final version of the manuscript.

References

[1] World Population Prospects: The 2019 Revision (XLS). Population Division of the Department of Economic and Social Affairs of the United Nations Secretariat. Available online: https://reliefweb.int/sites/reliefweb.int/files/resources/WPP2019_Highlights.pdf.

[2] UNESCO World Water Assessment Program. The United Nations World Water Development Report 2019: Leaving No One Behind. Available online: https://en.unesco.org/themes/water-security/wwap/wwdr/2019.

[3] Vikesland, P.J. Nanosensors for water quality monitoring. Nat. Nanotechnol, 13, 651–660 (2018).

[4] Gunasekaran, D.; Gerchman, Y.; Vernick, S. Electrochemical Detection of Waterborne Bacteria Using Bi-Functional Magnetic Nanoparticle Conjugates. *Biosensors* **2022**, *12*, 36. https://doi.org/10.3390/bios12010036.

[5] Rompre, A.; Servais, P.; Baudart, J.; de-Roubin, M.-R.; Laurent, P. Detection and enumeration of coliforms in drinking water: Current methods and emerging approaches. J. Microbiol. Methods 2002,49, 31–54.

[6] Alvarez, A.; Hernandez-Delgado, E.A.; Toranzos, G.A. Advantages and Disadvantages of Traditional and Molecular Techniques Applied to the Detection of Pathogens in Waters. *Water Sci. Technol.* **1993**, *27*, 253–256.

[7] P. Kumar, V. Kumar, J.S. Roy, Design of quad core photonic crystal fibers with flattened zero dispersion, Int. J. Electron. Commun. 98 (2019) 265–272.

[8] C.S. Kumar, R. Anbazhagan, Investigation on chalcogenide and silica based photonic crystal fibers with circular and octagonal core, Int. J. Electron. Commun. 72 (2017) 40–45.

[9] S. Luke, S. Sudheer, V.M. Pillai, Modeling and analysis of a highly birefringent chalcogenide photonic crystal fiber, Optik 126 (23) (2015) 3529–3532.

[10] K. Saitoh, M. Koshiba, Single-polarization single-mode photonic crystal fibers, IEEE Photon. Technol. Lett. 15 (10) (2003) 1384–1386.

[11] Anurag Upadhyay, Shivam Singh, Divya Sharma, Sofyan A. Taya, "A highly birefringent bend insensitive porous core PCF for endlessly single-mode operation in THz regime: An analysis with core porosity", Applied nanoscience, Vol. 11, No. 3, 1021–1030, 2021. DOI: 10.1007/s13204-020-01664-9

[12] Anurag Upadhyay, Shivam Singh, Divya Sharma, Sofyan A. Taya, "Analysis of Proposed PCF with Square Air Hole for Revolutionary High Birefringence and Nonlinearity", Photonics and Nanostructures - Fundamentals and Applications, Vol. 43, February 2021, article 100896. https://doi.org/10.1016/j.photonics.2021.100896

[13] Anurag Upadhyay, Shivam Singh, Divya Sharma, Sofyan A. Taya, "An Ultra-High Birefringent and Nonlinear Decahedron Photonic Crystal Fiber Employing Molybdenum Disulphide (MoS_2): A Numerical Analysis", Materials Science and Engineering B, Vol. 270, August 2021, article 115236. https://doi.org/10.1016/j.mseb.2021.115236

[14] Anurag Upadhyay, Shivam Singh, Divya Sharma, Sofyan A. Taya, "A comprehensive study of large negative dispersion and highly nonlinear perforated core PCF: theoretical insight", Physica Scripta, *Phys. Scr.* Vol. 97, 065504, (2022). https://doi.org/10.1088/1402-4896/ac6d1a

[15] J. Anthony, R. Leonhardt, A. Argyros, M.C. Large, Characterization of a microstructured Zeonex terahertz fiber, JOSA B 28 (5) (2011) 1013–1018.

[16] M.F.H. Arif, M.M. Hossain, N. Islam, S.M. Khaled, A nonlinear photonic crystal fiber for liquid sensing application with high birefringence and low confinement loss, Sens. Biosens. Res. 22 (2019), 100252.

[17] M.J.B.M. Leon, M.A. Kabir, Design of a liquid sensing photonic crystal fiber with high sensitivity, bireferingence & low confinement loss, Sens. Biosens. Res. 28 (2020) 1–7, 100335.

[18] M.M. Hasan, S. Sen, M.J. Rana, B.K. Paul, M.A. Habib, G.M. Daiyan, K. Ahmed, Heptagonal Photonic Crystal Fiber Based Chemical Sensor in THz Regime, 2019 Joint 8th International

Conference on Informatics, Electronics & Vision (ICIEV) and 2019 3rd International Conference on Imaging, Vision & Pattern Recognition (icIVPR), IEEE, 2019, pp. 40–44.
[19] B. Abdullah Al-Mamun, H.M.D. Bellal, D. Rahul, H. Mahadi, Zeonex-based tetra-rectangular core-photonic crystal fiber for NaCl detection, Nanosci. Nanotechnol. 10 (2020) 1–9.
[20] F.A. Mou, M.M. Rahman, M.R. Islam, M.I.H. Bhuiyan, Development of a photonic crystal fiber for THz wave guidance and environmental pollutants detection, Sens. Biosens. Res. 29 (2020), 100346.
[21] F. Iqbal, S. Biswas, A.A.-M. Bulbul, H. Rahaman, B.M. Hossain, E.M. Rahaman, A. M. Awal, Alcohol sensing and classification using PCF-based sensor, Sens. Biosens. Res. (2020), 100384, https://doi.org/10.1016/j.sbsr.2020.100384.
[22] Etu Podder, Md. Bellal Hossain, Md. Ekhlasur Rahaman, Abdullah Al-Mamun Bulbul, Kawsar Ahmed, "Design and optimization of terahertz blood components sensor using photonic crystal fiber", Sensing and Bio-Sensing Research 30, 100386 (2020).
[23] Mahmoud M. A. Eid, Ahmed Nabih Zaki Rashed, Abdullah Al-Mamun Bulbul, Etu Podder, "Mono-Rectangular Core Photonic Crystal Fiber (MRC-PCF) for Skin and Blood Cancer Detection", Plasmonics, https://doi.org/10.1007/s11468-020-01334-0
[24] K. Ahmed, M. Morshed, S. Asaduzzaman, M.F.H. Arif, Optimization and enhancement of liquid analyte sensing performance based on square-cored octagonal photonic crystal fiber, Optik 131 (2017) 687–696.
[25] M.F.H. Arif, K. Ahmed, S. Asaduzzaman, M.A.K. Azad, Design and optimization of photonic crystal fiber for liquid sensing applications, Photon. Sens. 6 (3) (2016) 279–288.
[26] B. Abdullah Al-Mamun, J. Rayhan Habib, D. Sumon Kumar, R. Tonmoy, S. Md. Avijit, H.Md. Bellal, PCF based formalin detection by exploring the optical properties in THz regime, Nanosci. Nanotechnol. 10 (2020) 1–8.
[27] Sofyan A. Taya, Dana N. Alhamss, Abdulkarem H. M. Almawgani, Ahmad Alzahrani, Ilhami Colak, Shobhit K. Patel, "Tuberculosis detection using a low-loss and highly sensitive photonic crystal fiber technique in the terahertz regime", Journal of the Optical Society of America B, J. Opt. Soc. Am. B Vol. 40, No. 9, 2382-2391 (2023). https://doi.org/10.1364/JOSAB.497918

[28] Abdulkarem H. M. Almawgani, Dana N. Alhamss, Sofyan A. Taya, Ayman Taher Hindi, Anurag Upadhyay, Shivam Singh, Ilhami Colak, Amrindra Pal, Shobhit K. Patel, "Identification of four detrimental chemicals using square-core photonic crystal fiber in the regime of THz", Journal of Applied Physics Vol. 133, No. 24, 243103 (2023). https://doi.org/10.1063/5.0152927
[29] Abdulkarem H. M. Almawgani, Dana N. Alhamss, Sofyan A. Taya, Ayman Taher Hindi, Anurag Upadhyay, Shivam Singh, Ilhami Colak, Amrindra Pal, Shobhit K. Patel, "Theoretical analysis of a refractive index sensor based on a photonic crystal fiber with a rectangular core", Optical and Quantum Electronics, Vol. 55, No. 10, Article number 881 (2023). https://doi.org/10.1007/s11082-023-05172-2
[30] Kuiri, B., Dutta, B., Sarkar, N. *et al.* Development of photonic crystal fiber supporting 124 OAM modes with flat dispersion and low confinement loss. *Opt Quant Electron* **54**, 527 (2022). https://doi.org/10.1007/s11082-022-03942-y

[31] Yundong Liu, Xili Jing, Hailiang Chen, Jianshe Li, Ying Guo, Song Zhang, Hongyu Li, Shuguang Li, "Highly sensitive temperature sensor based on sagnac interferometer using photonic crystal fiber with circular layout", Sensors and Actuators A: Physical, Volume 314, 112236 (2020). https://doi.org/10.1016/j.sna.2020.112236
[32] A. Ghazanfari, W. Li, M.C. Leu, G.E. Hilmas, A novel freeform extrusion fabrication process for producing solid ceramic components with uniform layered radiation drying, Addit. Manuf. 15 (2017) 102–112.
[33] A.M. Cubillas, S. Unterkofler, T.G. Euser, B.J. Etzold, A.C. Jones, P.J. Sadler, P. Wasserscheid, P.S.J. Russell, Photonic crystal fibres for chemical sensing and photochemistry, Chem. Soc. Rev. 42 (22) (2013) 8629–8648.

[34] V. Kaur, S. Singh, Extremely sensitive multiple sensing ring PCF sensor for lower indexed chemical detection, Sens. Biosens. Res. 15 (2017) 12–16.
[35] H. Ebendorff-Heidepriem, J. Schuppich, A. Dowler, L. Lima-Marques, T.M. Monro, 3D-printed extrusion dies: a versatile approach to optical material processing, Opt. Mater. Express 4 (8) (2014) 1494–1504.
[36] Abdullah Al-Mamun Bulbul, Hasibur Rahaman, Sandipa Biswas, Md Bellal Hossain, Abdullah-Al Nahid, Design and numerical analysis of a PCF-based bio-sensor for breast cancer cell detection in the THz regime, Sensing and Bio-Sensing Research, Volume 30, 2020, 100388.
[37] M.A. Habib, M.S. Anower, L.F. Abdulrazak, M.S. Reza, Hollow core photonic crystal fiber for chemical identification in terahertz regime, Opt. Fiber Technol. 52 (2019) 101933.
[38] Seemesh Bhaskar, Adarsh Kumar Singh, Pratyusha Das, Palash Jana, Sriram Kanvah, Shivakiran Bhaktha B N, and Sai Sathish Ramamurthy, "Superior Resonant Nanocavities Engineering on the Photonic Crystal-Coupled Emission Platform for the Detection of Femtomolar Iodide and Zeptomolar Cortisol", *ACS Applied Materials & Interfaces 12* (30), 34323-34336 (2020). DOI: 10.1021/acsami.0c07515.

[39] Xiong Y, Shepherd S, Tibbs J, Bacon A, Liu W, Akin LD, Ayupova T, Bhaskar S, Cunningham BT. Photonic Crystal Enhanced Fluorescence: A Review on Design Strategies and Applications. *Micromachines*. 2023; 14(3):668. https://doi.org/10.3390/mi14030668

[40] Jibon, R. H., Rahaman, Md. E., & Alahe, M. A. "Detection of primary chemical analytes in the THz regime with photonic crystal fiber". *Sensing and Bio-Sensing Research*, *33*, 100427 (2021). https://doi.org/10.1016/j.sbsr.2021.100427
[41] Jibon, R. H., Ahmed, M., & Hasan, Md. K. "Identification of detrimental chemicals of plastic products using PCF in the THz regime". *Measurement: Sensors*, *17*, 100056 (2021). https://doi.org/10.1016/j.measen.2021.100056
[42] Abdullah-Al-Shafi, Md., & Sen, S. "Design and analysis of a chemical sensing octagonal photonic crystal fiber (O-PCF) based optical sensor with high relative sensitivity for terahertz (THz) regime". *Sensing and Bio-Sensing Research*, *29*, 100372 (2020). https://doi.org/10.1016/j.sbsr.2020.100372
[43] bin Murshed Leon, M. J., Abedin, S., & Kabir, M. A. "A photonic crystal fiber for liquid sensing application with high sensitivity, birefringence and low confinement loss". *Sensors International*, *2*, 100061 (2021). https://doi.org/10.1016/j.sintl.2020.100061
[44] Hossain, Md. S., & Sen, S. "Design and Performance Improvement of Optical Chemical Sensor Based Photonic Crystal Fiber (PCF) in the Terahertz (THz) Wave Propagation". *Silicon*, *13*(11), 3879–3887 (2021). https://doi.org/10.1007/s12633-020-00696-8

Paper title: Numerical analysis of a photonic crystal fiber-based biosensor for the detection of Vibrio Cholera, and Escherichia Coli bacteria in the THz regime

A PCF sensor is proposed for detecting two types of waterborne bacteria. The core region is made up of a single rectangle and the cladding has 32 rectangular air holes. Zeonex is employed as the fiber material. Using Comsol 5.6, the model is numerically analyzed and structured. Extremely high relative sensitivity (97.996%) is obtained which indicate an efficient PCF sensor.